***Title***

*National-scale assessment of decadal river migration at critical bridge infrastructure in the Philippines*

***Author names and affiliations***

Richard J Boothroyd (0000-0001-9742-4229)

School of Geographical and Earth Sciences, University of Glasgow, United Kingdom

Richard D Williams (0000-0001-6067-1947)

School of Geographical and Earth Sciences, University of Glasgow, United Kingdom

Trevor B Hoey (0000-0003-0734-6218)

Department of Civil and Environmental Engineering, Brunel University London, United Kingdom

Pamela LM Tolentino (0000-0002-1803-9734)

National Institute of Geological Sciences, University of Philippines, Philippines

Xiao Yang (0000-0002-0046-832X)

Department of Geological Sciences, University of North Carolina, United States

**Corresponding author**

Richard J Boothroyd (richard.boothroyd@glasgow.ac.uk)

## Highlights

- River migration poses a geomorphic hazard to bridges
- Google Earth Engine workflow automates measurement of decadal planform adjustment
- Analyses reveal the diversity of river planform adjustment across the Philippines
- Planform adjustment is local and spatially heterogeneous in nature
- Magnitude of adjustment implies bridge design should accommodate channel dynamism


## Abstract

River migration represents a geomorphic hazard at sites of critical bridge infrastructure, particularly in rivers where migration rates are high, as in the tropics. In the Philippines, where exposure to flooding and geomorphic risk are considerable, the recent expansion of infrastructural developments warrants quantification of river migration in the vicinity of bridge assets. We analysed publicly available bridge inventory data from the Philippines Department of Public Works and Highways (DPWH) to complete multi-temporal geospatial analysis using three decades worth of Landsat satellite imagery in Google Earth Engine (GEE). For 74 large bridges, we calculated similarity coefficients and quantified changes in width for the active river channel (defined as the wetted channel and unvegetated alluvial deposits) over decadal and engineering (30-year) timescales. Monitoring revealed the diversity of river planform adjustment at bridges in the Philippines (including channel migration, contraction, expansion and avulsion). The mean Jaccard index over decadal (0.65) and engineering (0.50) timescales indicated considerable planform adjustment throughout the national-scale inventory. However, planform adjustment and morphological behaviour varied between bridges. For bridges with substantial planform adjustment, maximum active channel contraction and expansion was equal to 25% of the active channel width over decadal timescales. This magnitude of lateral adjustment is sufficient to imply the need for bridge design to accommodate channel dynamism. For other bridges, the planform remained stable and changes in channel width were limited. Fundamental differences in channel characteristics and morphological behaviours emerged between

different valley confinement settings, and between rivers with different channel patterns, indicating the importance of the local geomorphic setting. We recommend satellite remote sensing as a low-cost approach to monitor river planform adjustment with large-scale planimetric changes detectable in Landsat products; these approaches can be applied to other critical infrastructure adjacent to rivers (e.g. road, rail, pipelines) and extended elsewhere to other dynamic riverine settings.

**Keywords**

*Fluvial geomorphology; geomorphic hazards; bridge scour; planform adjustment; Google Earth Engine; river erosion; river deposition; Philippines*

## Graphical abstract

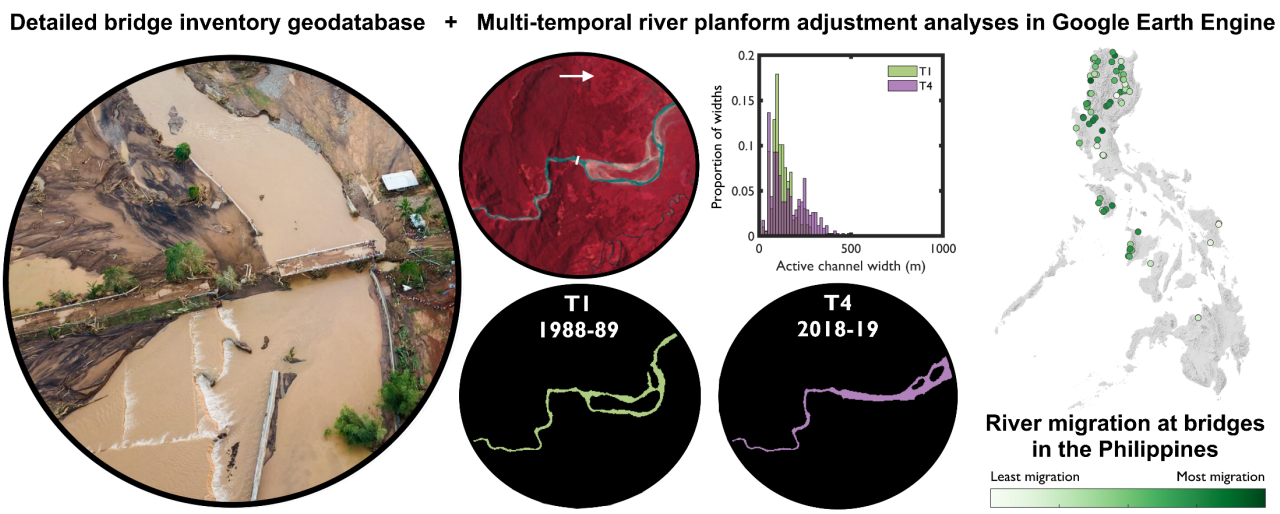

## 1. Introduction

Rivers and their floodplains are dynamic in space and time, whereas bridges and their foundations are fixed in position (Arneson et al., 2012). River bridges are vulnerable nodes in transport and utility networks that are exposed to flood-related hazards more than other forms of infrastructure (Pregnolato, 2019). Additional to flood-related hazards, geomorphic hazards such as river instability can damage or lead to the costly failure of river bridges (Cotton, 1999; Johnson and Whittington, 2011). The economic costs associated with bridge failure are high; when including the secondary costs additional to bridge repair, the total average cost for a single bridge failure in the USA is estimated to be US$13 million (Enke et al., 2008; Briaud et al., 2014). The failure of bridges can also cause lengthy interruptions to connections between communities; for example in the Philippines, the replacement of the Bintacan bridge following Typhon Lewin (2016) has taken more than three years to complete, with an economic cost of US$2 million (DPWH Regional Office II, 2020). River reaches adjust to imposed flow, sediment and vegetation conditions across vertical and/or lateral dimensions (Brierley and Fryirs, 2005; Fryirs 2017). With respect to bridges, vertical adjustment leads to either scour to bridge piers or aggradation which causes subsequent loss of below deck conveyance capacity and increases the risk of structural damage during high flows. Lateral adjustment occurs either as channel migration, expansion, contraction, or avulsion which poses a risk to bridge abutments and/or the viability of the bridge as a crossing.

Scour is cited as the most common cause of bridge failure at river crossings worldwide (Kirby et al., 2015). General scour occurs irrespective of the existence of a bridge, whereas local and contraction scour are directly attributable to the effects of the bridge (Coleman and Melville, 2001; Wang et al., 2017). General scour includes the removal of erodible sediment through lateral and vertical adjustment processes, operating over timescales of several years or longer (Coleman and Melville, 2001). Although it has received less attention than local and contraction scour (Johnson and Whittington, 2011), general scour can be equally damaging by modifying the angle of flow attack, accentuating local and contraction scour, undermining or outflanking bridge approaches (resulting in bridge redundancy) and reducing flow

conveyance at bridge openings (due to flow misalignment and sediment deposition; Melville and Coleman, 2000; Lagasse et al., 2004).

Planform adjustment can have significant consequences if not allowed for in the design of new bridges and in the implementation of countermeasures at existing bridges (Melville and Coleman, 2000; Arneson et al., 2012). Remedial actions (e.g. guide banks or bank protection) become increasingly difficult and expensive as flow alignment deteriorates. Monitoring of planform adjustments and the prediction of future river migration is integral for infrastructure developments in dynamic riverine settings (Mosselman, 2006; Best et al., 2007). A well-documented example is the 4.8 km Bangabandhu Multipurpose Bridge (Jamuna Bridge) on the Jamuna River, Bangladesh. This bridge is positioned where a dynamic braid-belt narrows so is susceptible to high rates of morphological change; this means that continued monitoring and sustained river engineering are necessary to ensure that the bridge is not outflanked (Best et al., 2007). Annual to inter-annual sequences of satellite imagery have been used to monitor bar morphodynamics and floodplain erosion in the vicinity of the bridge (Best et al., 2007; Islam et al., 2017). Similar monitoring has been undertaken along large bridges on the Padma River, Bangladesh (McLean et al., 2012) and Ayeyarwady River, Myanmar (Oo et al., 2019). These efforts are particularly important at sites with anthropogenic interventions (such as river training and bank protection measures) where flow patterns are modified (Baki and Gan, 2012) and scour effects can be greater.

Although lateral channel adjustment poses risks to critical bridge infrastructure, few studies have leveraged freely available satellite imagery and cloud-based computing platforms to assess river migration at sites of critical bridge infrastructure. Google Earth Engine (GEE), a cloud-based computing platform for planetary-scale geospatial analyses (Gorelik et al., 2017), allows users to take their own algorithms to petabytes worth of geospatial data (Wulder and Coops, 2014). With access to medium resolution satellite imagery spanning engineering timescales (e.g. Landsat products), multi-spectral bands (e.g. near-infrared and short-wave infrared) allow for calculation of multi-spectral indices, useful for indicating the relative abundance of features of interest in support of highly differentiated fluvial geomorphology applications (Spada et al., 2018). Image compositing (aggregations of spatially overlapping images) help to optimally resolve exposed in-channel sediment, provide consistent estimates of bankfull channel planform and integrate planform

changes over consistent time intervals (Schwenk et al., 2017). Combined, these features allow for multi-temporal analysis of the wider dynamics of fluvial systems (including water, sediment and vegetation; Boothroyd et al., 2020) enabling planform adjustments at sites of critical bridge infrastructure to be quantitatively assessed.

In the Philippines, the road network handles 90% of passenger and 50% of freight transportation (Vallejo, 2015) and is vital for linking rural communities (Olssen, 2009). In nominal terms, public infrastructure expenditure increased by 41.8% year-on-year in the first half of 2018 (World Bank, 2018) and as part of accelerated public spending, the Department of Public Works and Highways (DPWH) reported that between 2016 and 2018, 120 new bridges were constructed and 204 existing bridges were replaced (DPWH, 2018). Rivers are particularly dynamic in the Philippines, with fluctuating sediment supply driven by monsoon and typhoon related landslides, earthquakes, volcanoes and anthropogenic activities including artificial alignment, confinement, gravel extraction and dam construction (Gran et al., 2011; Catane et al., 2012; Gob et al., 2016). With high sediment supply from catchment headwaters, substantial channel migration rates (> 300 m per decade) have been reported (Dingle et al., 2019). This is exemplified where Typhoon Lawin (2016) mobilised large quantities of coarse sediment that led to channel re-organisation, bank erosion and damage to a major road bridge in the Bintacan catchment of the Cagayan Valley, Luzon (Dingle et al., 2019). Similar processes during Typhoon Urduja (2017) caused substantial infrastructural damages on Biliran Island (Visayas), including the failure of Caraycaray Bridge (Figure 1a and b). Repeat satellite imagery before and after the event show large-scale geomorphic changes including the activation of a flood channel and reworking of floodplain sediments, resulting in flow misalignment at the bridge opening (Figure 1c). With considerable exposure to flooding and geomorphic risk, and the recent expansion of infrastructural development, the Philippines presents a unique and timely opportunity to assess planform adjustment at sites of critical bridge infrastructure.

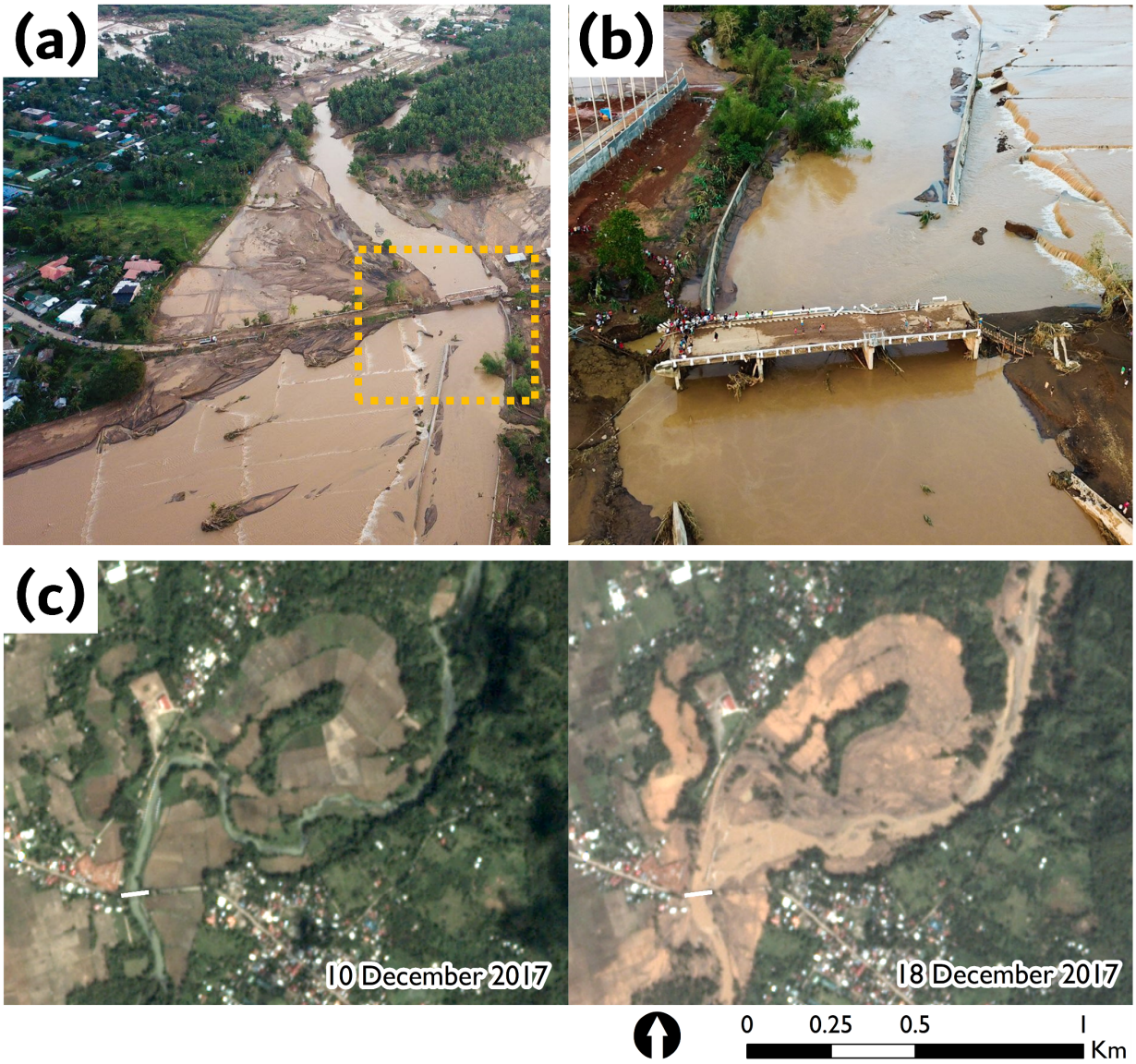


133

134 **Figure 1 –** Example of damages to infrastructure associated with flooding and geomorphic hazards in the
135 Philippines. Damage associated with Typhoon Urduja (2017) on Biliran Island (Visayas) at Caraycaray Bridge
136 (11°33'21.8"N 124°24'40.3"E; (a) and (b)). Note that image (b) is the upstream view of the dashed box in
137 (a). Repeat satellite imagery at Caraycaray Bridge shows large-scale geomorphic change immediately
138 upstream of the bridge (c). Caraycaray Bridge represented by the white line, flow direction is from north to
139 south and PlanetScope satellite imagery (3 m spatial resolution) was acquired before and after Tyhoon
140 Urduja (Planet Team, 2017).

141 In this paper we monitor river migration in the vicinity of critical bridge infrastructure in the Philippines.
142 Taking a two-dimensional planimetric perspective, we identify the physical boundaries of the active river
143 channel as the bankfull channel extent (Schumann et al., 2009; Rowland et al., 2016) and assess active river

channel change (i.e. planform adjustments). We present a national-scale, multi-temporal assessment of river migration at large bridges (> 200 m bridge deck length) through analysis of publicly available bridge inventory data from the DPWH and multi-temporal geospatial analysis using medium resolution satellite imagery (30 m spatial resolution) within Google Earth Engine (GEE). Data uncertainties arise as a function of sensor resolution relative to the size of the object of interest so analyses were limited to large bridges where the active river channel could be adequately resolved. Specifically, we extract binary active river channel masks of the bankfull extent (including the wetted channel and unvegetated, alluvial deposits) from Landsat products (Landsat 5, 7 and 8) using multi-spectral indices, before identifying planform adjustments over decadal and engineering (30-year) timescales. Similarity coefficients are calculated between successive active river channel masks to indicate river migration. Spatiotemporal quantification of active river channel width changes using RivWidthCloud (Yang et al., 2019) provide insight into the morphological processes acting at each river bridge. To further illustrate the typical range of channel behaviours (channel expansion, negligible morphological change and channel contraction), detailed analysis is reported at three bridge locations with distinct geomorphic settings. We do not seek here to make causal explanations of river adjustment or provide predictions of the magnitude of river migration at specific sites. Rather, we suggest that multi-temporal analysis from satellite remote sensing offers a low-cost approach for monitoring the relative risk of river migration at critical bridge infrastructure; the approach can be extended to include other infrastructure adjacent to rivers (e.g. rail and road) and applied across various dynamic riverine settings.

## 2. Methods

### 2.1. Construction of a geospatial bridge database

#### 2.1.1. Bridge characteristics

A geospatial database of Philippine bridges was retrieved from the Detailed Bridge Inventory Application (DPWH, 2020). Within the database, a bridge is defined as a structure carrying a road over a waterway, road or other feature, with a clear span of 3 meters or more between the inside faces of supports. Retrieved in April 2020, the database contained geospatial information for 8410 bridges along national roads, with attribute data including bridge deck length, year of construction and road type. Bridge locations were provided as latitude/longitude coordinates. The database was filtered to include only permanent bridges where the bridge deck length was equal to or greater than 200 m ($n$ = 256). A visual inspection was performed to ensure that bridges were located at contemporary river crossings ($n$ = 182) and only those bridges where the active channel width exceeded 150 m (equivalent to five Landsat pixels) were retained for analysis ($n$ = 74).

#### 2.1.2. Stream network configuration and geomorphic setting

A nationwide digital elevation model (DEM) acquired in 2013 and generated through airborne Interferometric Synthetic Aperture Radar (IfSAR), with a 5 m spatial resolution and 1 m root-mean-square error vertical accuracy (Grafil and Castro, 2014) was used for topographic analysis and extraction of the stream network. Bed elevations were extracted from the DEM at bridge points and appended to the geospatial database. The DEM was resampled to a 30 m spatial resolution (due to processing constraints) with TopoToolbox (Schwanghart and Scherler, 2014) used to hydrologically correct and extract the stream network using standard flow-routing algorithms. Bridge points were snapped to the stream network, with the upstream area, channel slope and Strahler stream order (Strahler, 1957) extracted at each point. Because channel slope was variable over short distances, slope values were averaged over 0.3 km segment lengths. To compare the position of bridges along stream networks of varying length, the position of the bridge point along the trunk stream was normalised as the trunk stream length to each bridge point

(distance along the stream network from the channel head to the bridge point), divided by the total trunk stream length (distance along the stream network from the channel head to the catchment outlet). Simple descriptions of the geomorphic setting in the vicinity of each bridge were appended to the geospatial database following a visual assessment of the most recently available Google Earth aerial imagery. Geomorphic descriptors included: confinement (confined, partly-confined or laterally unconfined; Brierley and Fryirs, 2005), number of channel threads (single or multiple) and channel pattern (straight, meandering, wandering or braided; after Church, 2006; Beechie et al., 2006).

### 2.2. Multi-temporal analysis of planform adjustment in Google Earth Engine

#### 2.2.1. Extracting active river channel masks

Google Earth Engine (GEE) was used to extract active river channel masks from Landsat 5, 7 and 8 satellite imagery. Landsat products were selected for their archive length from 1970 to present day and repeat global coverage (Smith and Pain, 2009), providing outputs at a spatial resolution of 30 m. The workflow is summarised in Figure 2, with three main processing steps: (i) cloud masking and temporal compositing; (ii) active river channel classification; and, (iii) cleaning and image export.

In the first processing step, a circular buffer with a user-defined radius was drawn around each bridge point. The buffer acts as a region of interest (ROI) to complete the subsequent analyses. The buffer extends in upstream and downstream directions around the bridge point; as river migration downstream of a bridge can extend back upstream toward the bridge reach (Lagasse et al., 2004). The user-defined radius was constant for all bridges (4.5 km) equal to approximately ten times the mean bridge length (see Section 2.2.4. for the rationale). For bridges located proximal to outlet points (e.g. ocean, lakes), the ROI was manually edited to include only the active river channel so excluding the large water bodies. Time filters were defined to select all available Landsat satellite imagery (Landsat 5, 7 and 8) for specified two-year time periods. The two-year time periods were selected to collect sufficient cloud-free images in a region where cloud cover can be persistent (Long and Giri, 2011). Decadal time intervals have previously been used to assess planform adjustments in Philippine river systems (Dingle et al., 2019). Image collections were automatically constructed for each of the specified time periods, with the CFmask algorithm applied

to each image in the collection to mask obstructions from cloud and cloud shadow pixels (Figure 2a; Foga et al., 2017). To generate a single image from the image collection, a median reducer was applied to aggregate all non-cloud pixels, generating a temporal composite for each spectral band (Figure 2b). The temporal composite is advantageous for overcoming data shortcomings associated with the scan line corrector (SLC) failure aboard Landsat 7 (Pringle et al., 2009), providing a cloud-free 'average' image.

In the second processing step, multi-spectral indices were used to classify the wetted channel and alluvial deposits from the temporal composite images, producing an intermediate binary active river channel mask (Figure 2c-e). The classification method of Zou et al., (2018) was used to classify water pixels, producing a binary water mask from the normalized difference vegetation index, NDVI (Rouse *et al*., 1974), the enhanced vegetation index, EVI (Huete et al., 2002) and the modified normalized difference water index, MNDWI (Xu, 2006). The same multi-spectral indices were used to classify alluvial deposits, with the active channel boundary enforced by excluding vegetated pixels. Active channel pixels were classified using relational operators where MNDWI $\geq$ -0.4 and NDVI $\leq$ 0.2. An NDVI threshold of 0.2 is established in the literature for dense riparian vegetation (Bertoldi et al., 2011). Binary wetted channel and alluvial deposit masks were combined (i.e. geometric union) to produce the intermediate binary active river channel mask.

In the final processing step, the intermediate binary mask was cleaned using standard image processing morphological operations. Disconnected areas containing less than 100 pixels were assumed to have been erroneously classified and removed (Figure 2g). A circular structuring element with a radius of three pixels performed a single iteration of morphological closing (binary image dilation followed by erosion) on the retained pixels (Figure 2h). Morphological closing eliminates small gaps, fuses narrow breaks and narrows the separation between nearby objects (Haralick et al., 1987), thereby smoothing edgelines to produce a continuous representation of the active river channel. The workflow provides a binary active channel mask in the vicinity of bridge points for each time period specified, exported to Google Drive as a GeoTIFF.

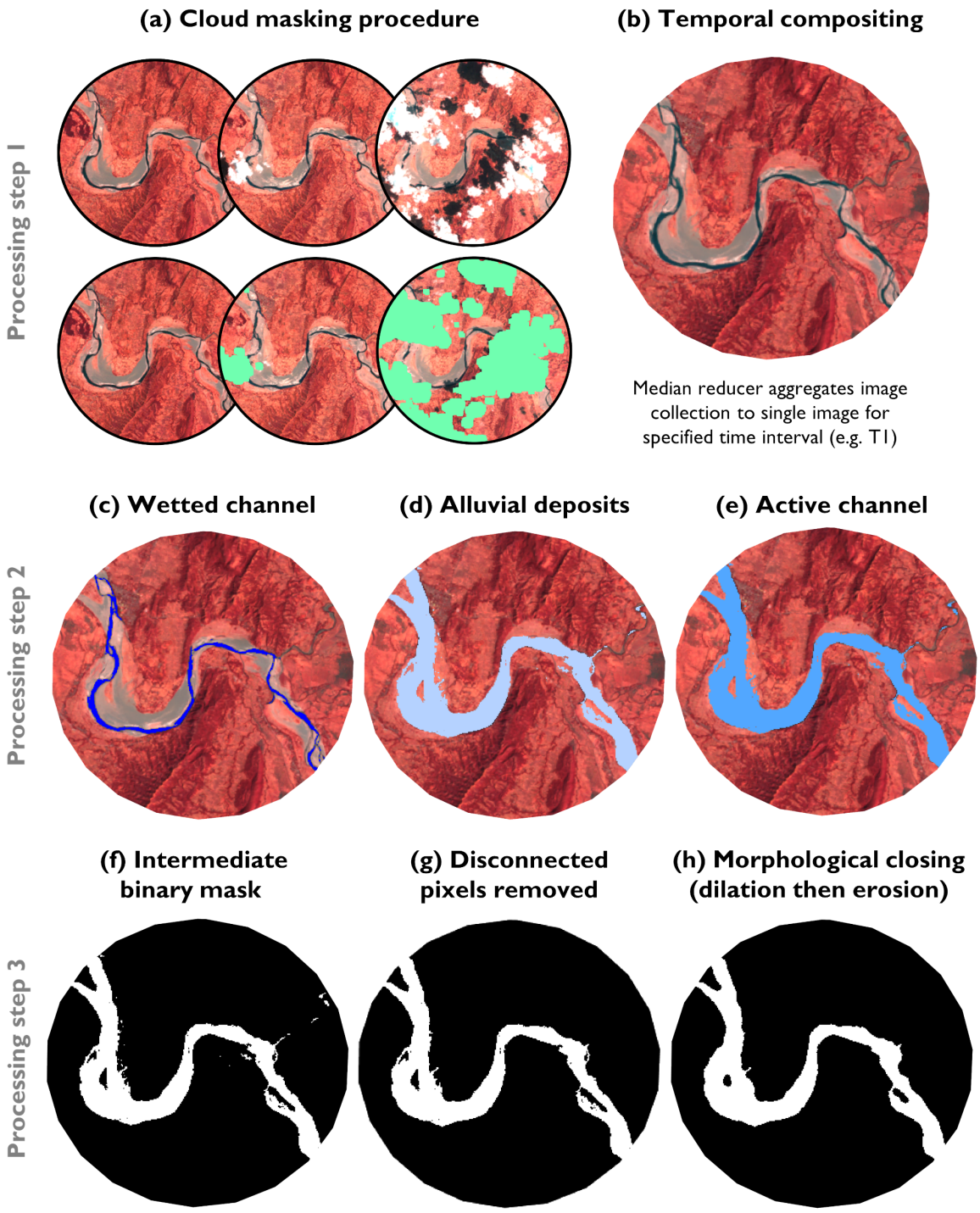


238

239 **Figure 2 –** Visual workflow for extracting the active river channel mask from a series of Landsat satellite
240 images in Google Earth Engine. ROI refers to the region of interest. Image collections contained all Landsat
241 imagery from 1st January to 31st December for the specified time period. Wetted channel classification
242 followed Zou et al., (2018), and alluvial deposits were classified using a relational operator where MNDWI ≥
243 -0.4 and NDVI ≤ 0.2. Threshold for removal of disconnected pixels was set to 100 pixels. Workflow shown

for the Sarrat Bridge (Padsan River; 18°08'15.5"N 120°40'02.9"E), base maps are false colour images using short-wave infrared, red and green bands.

### 2.2.2. Accuracy assessment of active river channel extraction

Following extraction of active river channel masks, accuracy assessment was undertaken on a 10% sample of the bridge inventory ($n$ = 7). The sample sites were randomly selected from the bridge inventory; their geographical coverage includes the island groups of Luzon and Visayas covering the full range of bridge lengths (range 262 to 1448 m) and ages (range 11 to 89 years). For each site, false colour temporal composites for the short-wave infrared, red and green bands were generated for the time periods 1988-89 (T1) and 2018-19 (T4), and the active river channel manually digitised in GIS. A number of factors affect the uncertainty of manual riverbank digitization including vegetation density, shadows and user inconsistences (see comprehensive list in Table 1 in Donovan et al., 2019). To minimise digitization (delineation) uncertainties, accuracy assessment was completed on temporal composite images to reduce any potential seasonal vegetation or river stage effects between images; arbitrary user inconsistency was limited by having a single user complete the manual digitization procedure. Using active channel shapefiles as the ground truth (validation) dataset, we examined the classification accuracy using precision ($P$), recall ($R$), and $Fl$ score. The approach follows Woznicki et al., (2019), but rather than counting the number of pixels to assess classification performance, we use the area of the active channel ($km^2$) due to differences in feature representation between datasets (ground truth = vectorized; classification = rasterized). Conversion from vector to raster (or vice-versa) would introduce additional error into the accuracy assessment. Precision, also known as positive predicted value, is the proportion of the classified dataset that is correct when compared against the ground truth dataset (Eq 1). Recall, also known as hit rate, is the proportion of the ground truth that has been correctly classified (Eq 2). $Fl$ measures classification accuracy by balancing precision and recall using their harmonic mean (Eq 3):

$$P = \frac{Tp}{Tp + Fp} \quad [1]$$

$$R = \frac{Tp}{Tp + Fn} \quad [2]$$

$$Fl = 2 * \frac{P * R}{P + R} \quad [3]$$

where $Tp$ is the area of true positives (areas correctly classified as the active channel), $Fp$ is the area of false positives (areas incorrectly classified as the active channel) and $Fn$ is the area of false negatives (areas incorrectly classified as non-active channel). From the ratio of $Fp$ to $Fn$, we calculated the error bias ($E$) following Wing et al., (2017). The error bias determines whether the classification underpredicts ($E < 1$) or overpredicts ($E > 1$) the active channel extent.

$$E = \frac{Fp}{Fn} \quad [4]$$

The GEE workflow performed well in classifying the active river channel (Table 1). The mean $Fl$ score was greater than 0.85 (both T1 and T4) and the mean recall rate indicates that we correctly identified more than 80% of the active river channel in the vicinity of critical bridge infrastructure (both T1 and T4). Performance metrics indicate that precision was greater than recall, and the error bias was consistently less than 0.5. A greater area of false negatives (incorrectly classifying an area as non-active channel) than false positives (incorrectly classifying an area as active channel) indicate that the GEE workflow generally underpredicted the active channel extent, and that this underprediction was consistent through time. Visual inspection of results from the accuracy assessment revealed that much of the underprediction occurred at the edges of the active channel (i.e. at the physical boundary of the river). Key sources of uncertainty in the classification are detailed in Section 4.4., but we suggest that patterns of river migration can be identified from the GEE workflow.

**Table 1 –** Active river channel classification accuracy assessments from sample bridge sites (*n* = 7). T1 (1988-89) and T4 (2018-19) refer to the time period of analysis.

| Bridge | T1 (1988-89) | | | | T4 (2018-19) | | | |
|---|---|---|---|---|---|---|---|---|
| | Precision | Recall | F1 | Error bias | Precision | Recall | F1 | Error bias |
| *Narciso Ramos* | 0.942 | 0.907 | 0.924 | 0.602 | 0.947 | 0.814 | 0.876 | 0.244 |
| *Cabagan-Sta.Maria* | 0.984 | 0.940 | 0.961 | 0.246 | 0.978 | 0.937 | 0.957 | 0.333 |
| *Jones* | 0.969 | 0.753 | 0.848 | 0.097 | 0.959 | 0.826 | 0.888 | 0.202 |
| *Lumintao* | 0.973 | 0.947 | 0.960 | 0.490 | 0.978 | 0.896 | 0.935 | 0.195 |
| *Sibalom* | 0.945 | 0.833 | 0.885 | 0.291 | 0.931 | 0.852 | 0.890 | 0.428 |
| *Naguilian* | 0.918 | 0.538 | 0.678 | 0.104 | 0.941 | 0.753 | 0.837 | 0.190 |
| *Bubulayan* | 0.957 | 0.729 | 0.827 | 0.120 | 0.955 | 0.792 | 0.866 | 0.180 |
| **Average** | 0.956 | 0.807 | 0.869 | 0.279 | 0.956 | 0.839 | 0.893 | 0.253 |

### 2.2.3. Similarity coefficients to indicate planform adjustment

Similarity coefficients between binary active channel masks were calculated in GEE to indicate planform adjustment. Similarity coefficients express the proportion of area that two objects possess mutually, compared to the total area possessed by one object, or the other, or both (Hohn, 1976). We applied similarity coefficients in binary presence-absence form, summing pairwise attribute comparisons between contingency tables (confusion matrix) of successive active channel binary masks (Figure 3).

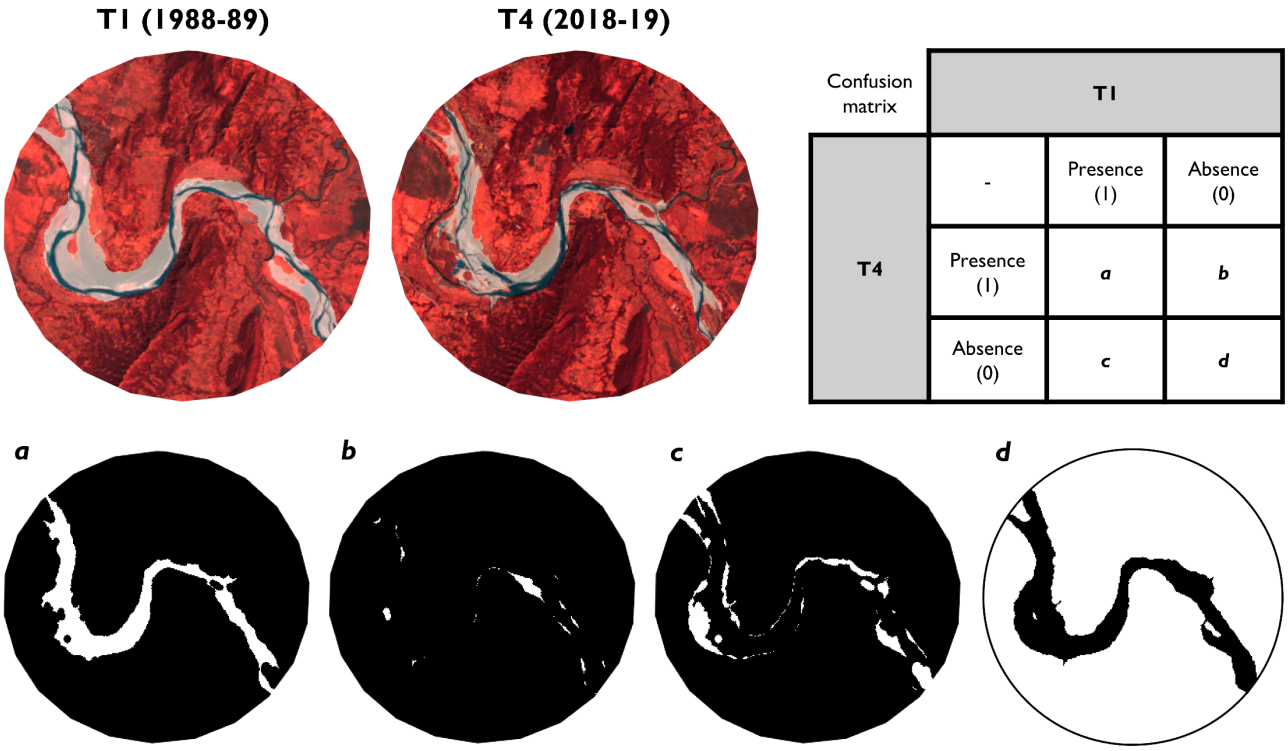


297

298 **Figure 3** – Schematic representation of the contingency table (confusion matrix) between T1 and T4 for the
299 Sarrat Bridge (Padsan River; 18°08'15.5"N 120°40'02.9"E). Binary active channel masks are overlaid on top
300 of the false colour composites to show active channel extents at T1 and T4. Contingency table shows the
301 definitions of *a* (presence-presence instances), *b* (absence-presence instances), *c* (presence-absence
302 instances) and *d* (absence-absence instances).

303

304 Although many objective and scale invariant binary similarity coefficients are available (e.g. Choi et al.,
305 2010); we selected similarity coefficients where negative matches (*d*) are excluded (Table 2), so not to
306 assess the similarity of non-river pixels. The Jaccard index is given by the intersection over union and has
307 been preferred when there are many presence-presence instances (Clifford and Stephenson, 1976). The
308 Jaccard index, also referred to as the Critical Success Index (CSI) or Threat Score ($F^{<2>}$), is an established
309 validation measure for assessing the spatial distribution of flooding between predicted and simulated
310 extents in hydrodynamic models (e.g. Horritt and Bates, 2001; Aronica et al., 2002). The Dice similarity
311 coefficient, also referred to as the F1 score, is similar in form to the Jaccard index but gives double weight
312 to presence-presence instances. It has been favoured for assessing the similarity of datasets where there

313 are fewer presence-presence instances (Boyce and Ellison, 2011). Since the Jaccard index and Dice
314 similarity coefficients are correlated (Choi et al., 2010), here we only present results for the Jaccard index
315 (to equally treat areas with no planform adjustment, erosion or deposition). We calculated contingency
316 tables using the instances of binary pixels between active channel masks for different time periods (Figure
317 3) and applied the expression shown in Table 2. The Jaccard index ranges between 0 and 1, whereby
318 calculated values closer to 1 indicate greater similarity between active river channel masks (i.e. less
319 planform adjustment).

320

321 **Table 2 –** Similarity coefficients for indicating planform change. Schematic representations of *a* (presence-
322 presence instances), *b* (absence-presence instances) and *c* (presence-absence instances) are shown in
323 Figure 3.

| Similarity coefficient | Expression | Range | Reference |
|---|---|---|---|
| **Jaccard index** | $SJ = aa+b+c$ | [0,1] | Jaccard (1901) |
| **Dice similarity coefficient *** | $SD = 2a2a+b+c$ | [0,1] | Dice (1945) |

324 *** Dice similarity coefficient is equivalent to the F1 score (Equation 3).**

325

326 **2.2.4. Jaccard index sensitivity to start date and region of interest radius**

327 To assess suitable values for the start date of multi-temporal analysis (defining the time periods of analysis)
328 and the radius of the ROI, sensitivity analysis was undertaken on the 10% sample of the bridge inventory (*n*
329 = 7). The start date was progressively shifted (S1 - S10; Figure 4a and b) and the radius of the ROI
330 incrementally increased from 1.5 to 6 km (1.5, 3, 4.5 and 6 km; Figure 4c and d). The Jaccard index was
331 calculated and then expressed in two forms; first calculated over the entire time range investigated (i.e.
332 reported as the Jaccard index between the initial (T1) and most-recent time interval (Tx)); then as the mean
333 value calculated over successive decades (i.e. the mean Jaccard index between T1 and T2, T2 and T3, T3
334 and T4).

Limited sensitivity to the start date of multi-temporal analysis is indicated by the variation in Jaccard index and mean Jaccard index (Figure 4 a and b). For the Lumintao Bridge (Mindoro Occidental, Luzon), the Jaccard index and the mean Jaccard index remain consistently high (range from 0.70 to 0.76 and 0.78 to 0.82), indicating insensitivity to the start date of multi-temporal analysis. In comparison, greater variation is expressed for the Jones Bridge (Isabela, Luzon), where the Jaccard index and mean Jaccard index are characterised by more intermediate values (range from 0.48 to 0.78 and 0.62 to 0.79). Across all start dates and for the sampled bridges, the average range in the Jaccard index is 0.17 and the average range in the mean Jaccard index is 0.12. To test whether the variance between start dates is greater than the variance for individual start dates, a non-parametric Kruskal-Wallis test was applied. The variance between start dates is not significantly greater than that for individual start dates at the 0.001 significance level. This limited sensitivity can in part be explained by the processes that govern planform adjustments; these processes are unlikely to occur uniformly through time reflecting natural variability in the time-series being inherent to fluvial systems. Intra-annual to inter-annual differences in the magnitude of geomorphic change processes make it unlikely that a dataset for a short river reach over the relatively short time period of satellite imagery will be stationary. However, if the sampled bridges were ranked by Jaccard index for each of the start dates, then the ranking would remain relatively consistent through time. Therefore, regardless of the selected start date, the timescales of interest (decadal and 30-year engineering) adequately capture the extended trajectory of planform adjustment.

Results are relatively insensitive to changes in the radius of the ROI, especially when the radius exceeds 3 km (Figure 4c and d). The smallest range in the Jaccard index is shown at the Narciso Ramos Bridge (Pangasinan, Luzon; range 0.20 to 0.26), where substantial planform adjustment is recorded irrespective of the radius of the ROI. For all sampled bridges, the mean average range in the Jaccard index is 0.15 and the average range in the mean Jaccard index is 0.10. To test whether the variance between different radii of ROI is greater than the variance for individual radii of ROI, the Kruskal-Wallis test is again applied. The variance between different radii of ROI is not significantly greater than that for individual radii of ROI at the 0.001 significance level. Reduced sensitivity to the radius of the ROI is explained by similar geomorphic processes operating over different lengths of the sampled river reaches. Given the scale of rivers analysed

362 in this application, a 4.5 km radius of the ROI is selected for subsequent analysis. The 4.5 km radius is equal
363 to approximately ten times the mean average bridge length.

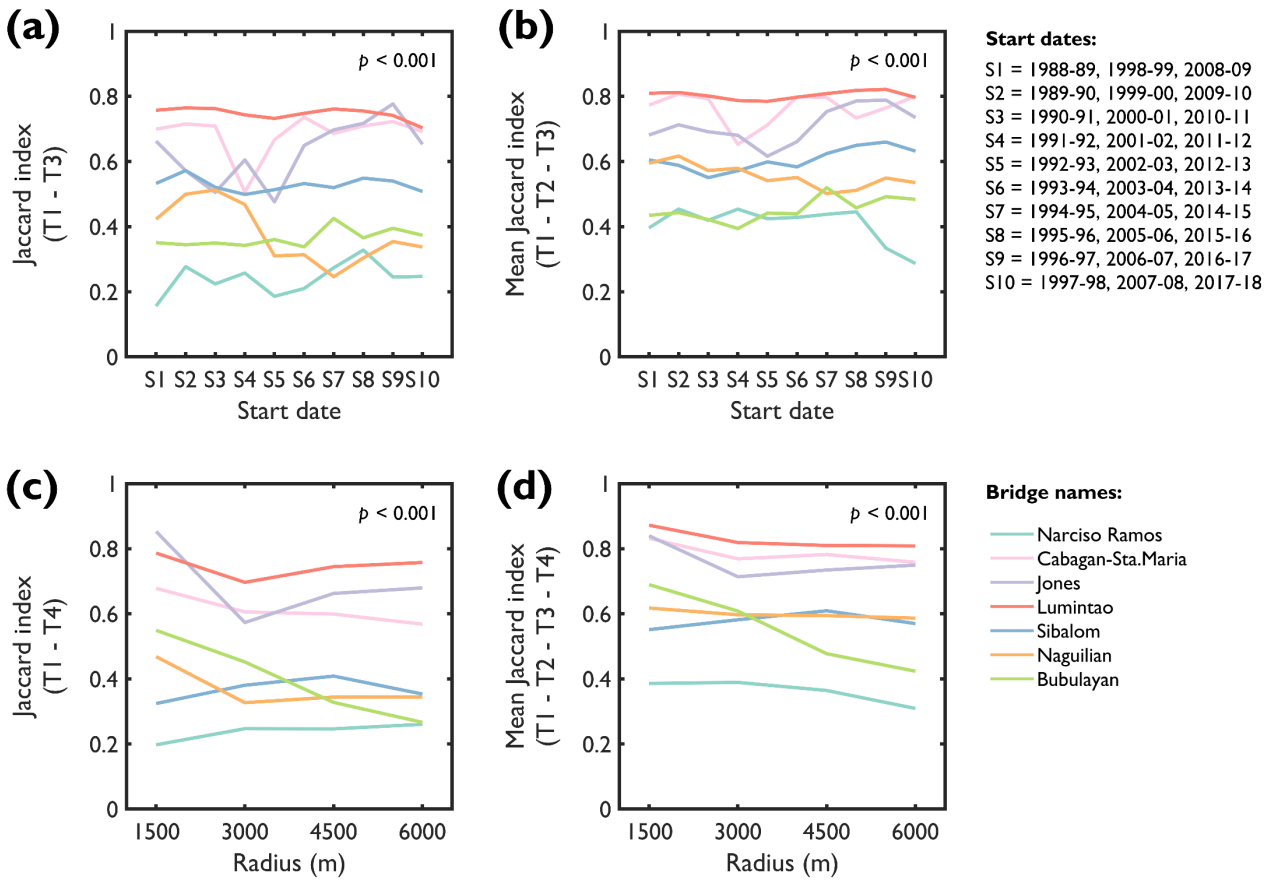

364

365 **Figure 4** – Sensitivity of the Jaccard index and mean Jaccard index to the start date (a-b); and radius of the
366 ROI (c-d) for sample bridge sites ($n$ = 7). $p$-values show the results of non-parametric Kruskal-Wallis tests; all
367 are statistically significant at the 0.001 significance level. The variance between start dates and radii of ROI
368 are not significantly greater than that at individual start dates, or for different radii of ROI.

369

370 For the results presented herein, GEE analyses were completed using a ROI with a radius of 4.5 km. Binary
371 active river channel masks were constructed and extracted from temporal composites covering a two-year
372 time period. Planform adjustment was assessed at decadal time intervals over the following periods: 1988-
373 89 (T1), 1998-99 (T2), 2008-09 (T3) and 2018-19 (T4). To indicate planform adjustment over 30-year
374 engineering timescales, the Jaccard index was calculated between T1 and T4; to indicate planform
375 adjustment over decadal timescales, the mean Jaccard index was calculated between T1 and T2, T2 and T3,

T3 and T4. We suggest that the spatial and temporal scales are appropriate to the geomorphic processes of interest and the overall trajectory of the system (i.e. appropriate for the amount of change being detected; Grabowski et al., 2014), but acknowledge that these values may not be universally applicable to river systems in different geographical settings.

#### 2.2.5. RivWidthCloud to quantify active river width

RivWidthCloud is an application in GEE for the extraction of river centreline and widths (Yang et al., 2019). The application can accurately estimate river widths from Landsat imagery, with computed widths closely matching *in situ* width measurements at gaging stations across the USA and Canada (Yang et al., 2019). Previous applications of RivWidthCloud have analysed only the wetted river channel. Here, we applied RivWidthCloud to analyse binary active channel masks around critical bridge infrastructure, for extraction of the active river channel centreline and width. The application remains unchanged from that reported in Yang et al., (2019) with binary active channel masks, rather than entire Landsat tiles, used as the input data. Based on sensitivity tests, user-defined parameters were set to 50 km, 10 pixels and 500 pixels for the maximum search distance, maximum island size and maximum branch length to remove. Application of RivWidthCloud returned spatially continuous active channel width estimates and centreline positions, with the mean average and standard deviation of active river channel width used in subsequent analysis. Given the lack of available field data for wetted and active river channel widths in the Philippines, we do not comment on the accuracy of computed RivWidthCloud width estimates.

## 3. Results

### 3.1. Bridge characteristics in the geospatial database

For the 74 bridges included in our analysis, bridge and stream network characteristics are shown in Figure 5. Bridges are distributed across the island groups of Luzon, Visayas and Mindanao, spanning 22 different provinces. More than 90% of the bridges were constructed since 1970 (Figure 5a), with an average bridge age of 30 years. To indicate the position of the bridge relative to the stream network, the normalised distance along the trunk stream was calculated (Figure 5b) ranging from 0 at the channel head to 1 at the catchment outlet. The normalised distance accounts for differences in trunk stream lengths (range 33 to 549 km). In general, bridges tend to be positioned closer to the catchment outlet, explained in part by the coastal highway configuration around NW Luzon which reflects the steep terrain further inland. Bridge lengths range from 200 to 1448 m (median = 365 m; mean = 437 m; standard deviation = 227 m; Figure 5c). The most common road type at the river crossings was primary (i.e. highway). Areas upstream of the bridge vary over three orders of magnitude (range 49 to 27447 $km^2$), with Strahler stream orders from three to seven (Figure 5d). Between bridges, the local channel slope varied by more than two orders of magnitude, from < 0.0001 to > 0.01 m/m (Supplementary materials). In terms of the local geomorphic setting, 54% of bridges were classified as partly-confined, 39% as laterally unconfined and 7% as confined. Channels were predominantly single-threaded (68%) as opposed to multi-threaded (32%). The full range of channel patterns were observed, including wandering (38%), meandering (35%), braided (22%) and straight (5%). The large bridges included in our geospatial database demonstrate a range of built characteristics, stream network configurations and geomorphic settings.

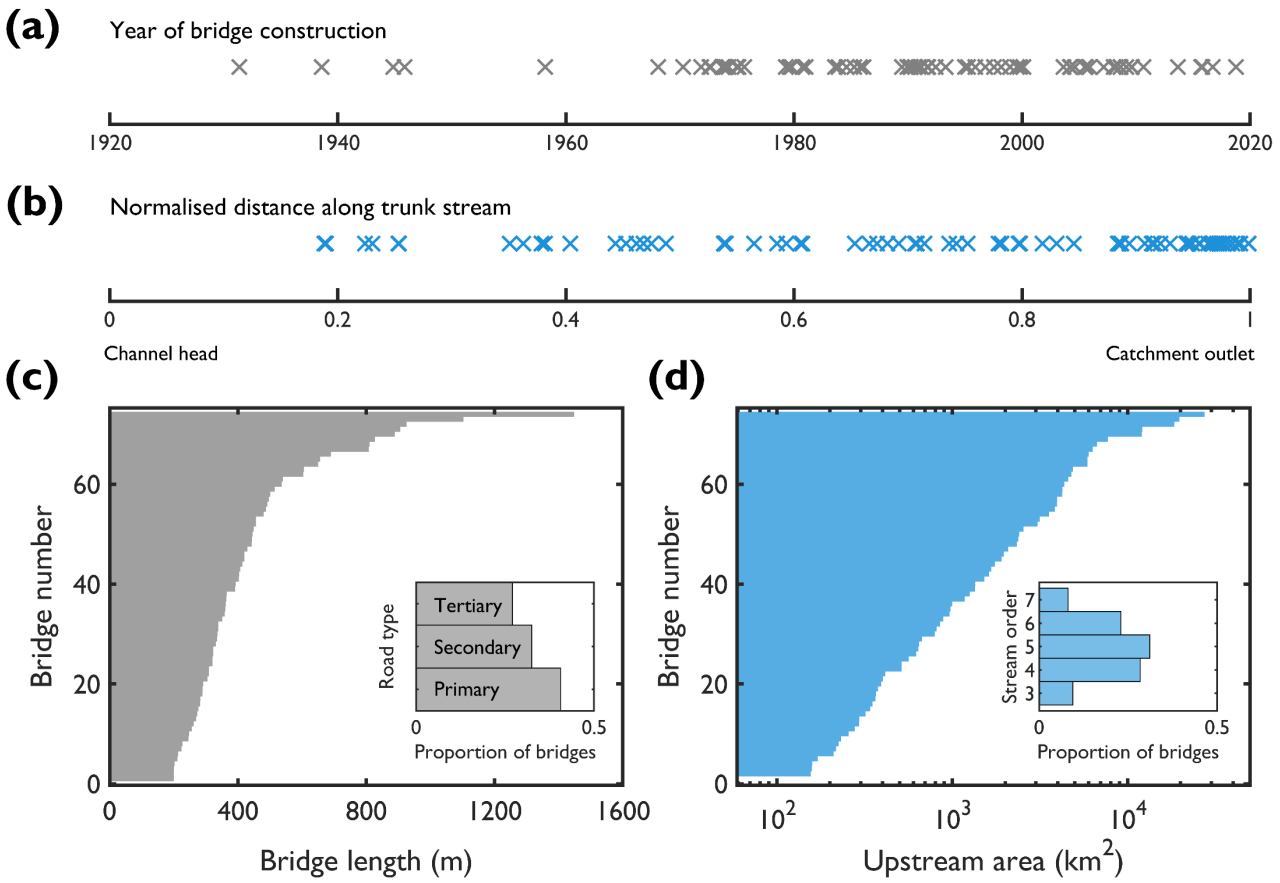


**Figure 5** – Bridge and stream network characteristics from the geospatial database ($n$ = 74). Year of bridge construction (a); bridge position as the normalised distance along the trunk stream (b); bridge length (c); and upstream area (d). Inset graphs in (c) and (d) show road types and Strahler stream orders.

### 3.2. National-scale assessment of planform adjustment at critical bridge infrastructure

Planform adjustment in the vicinity of large bridges varies across the Philippines in our national-scale analysis (Table 2 and Figure 6). Over the 30-year engineering timescale (Figure 6a), the mean Jaccard index is 0.50 (median = 0.49), indicating considerable planform adjustment at sites of critical bridge infrastructure. However, the spread of the 25$^{th}$ and 75$^{th}$ percentiles (50% of values in the range 0.30 to 0.66) and standard deviation of the Jaccard index (0.22) show substantial variation among bridge sites. Likewise, over decadal timescales (Figure 6b) the mean Jaccard index is 0.65 (median = 0.66), indicating marked planform adjustment over relatively short timescales. The decadal values are also characterised by variation (50% of values in the range 0.53 to 0.79; standard deviation = 0.17). Spatially, no geographic trend

in planform adjustment is seen across different islands, or for different regions (Figure 6a and b). The marked variation in planform adjustment between bridge sites, over engineering and decadal timescales, indicates a non-uniform response across the Philippines (i.e. different rivers experienced different extents of planform adjustment). An additional temporal component of analysis is added when looking at the range in the mean Jaccard index (Figure 6c). Although rivers at some bridge sites respond consistently through time (characterised by small ranges in the mean Jaccard index, as low as 0.01), other bridge sites experienced planform adjustments more inconsistently (characterised by large ranges in the mean Jaccard index, as high as 0.39). Bridge sites with larger ranges in mean Jaccard index indicate that planform adjustments did not occur uniformly through time. Combined, the Jaccard index, mean Jaccard index and range in mean Jaccard index suggest that river planform adjustment response varies across bridge sites in the Philippines.

Variation in active river channel widths, and changes in the active channel width through time, are also apparent at the national-scale. With RivWidthCloud used to quantify active channel width (Table 3 and Figure 6d), the average active channel width in the vicinity of large bridges is 273.9 m (median = 233.7 m); but this varies over an order of magnitude (range 79.4 to 763.2 m). 50% of bridges have an active channel width in the range 160.0 to 381.2 m. Temporally, minor changes in active channel width are shown in the vicinity of most bridges, but more substantial width changes are seen for some outliers (Figure 6e). Although the average change in active channel width across all sites is small (mean = -4.7 m; median = -4.3 m; 50% of values in range -13.4 to +8.6 m), outliers are represented by large width changes (up to -105.2 m of channel contraction, and up to +109.5 m of channel expansion). To account for the variation in active channel widths between different bridge sites, changes in width are normalised by active channel width (Figure 6f). Across all sites, the average normalised change is small (mean = -1.5%; median -1.9%; 50% of values in range -6.3 to +3.7%), but outliers show substantial geomorphic change, with active channel contraction and expansion equal to approximately 25% of channel width (maximum contraction = -25.3%, maximum expansion = 24.0%). Like planform adjustment, a diverse range of active channel width responses are shown at bridge sites in the Philippines.

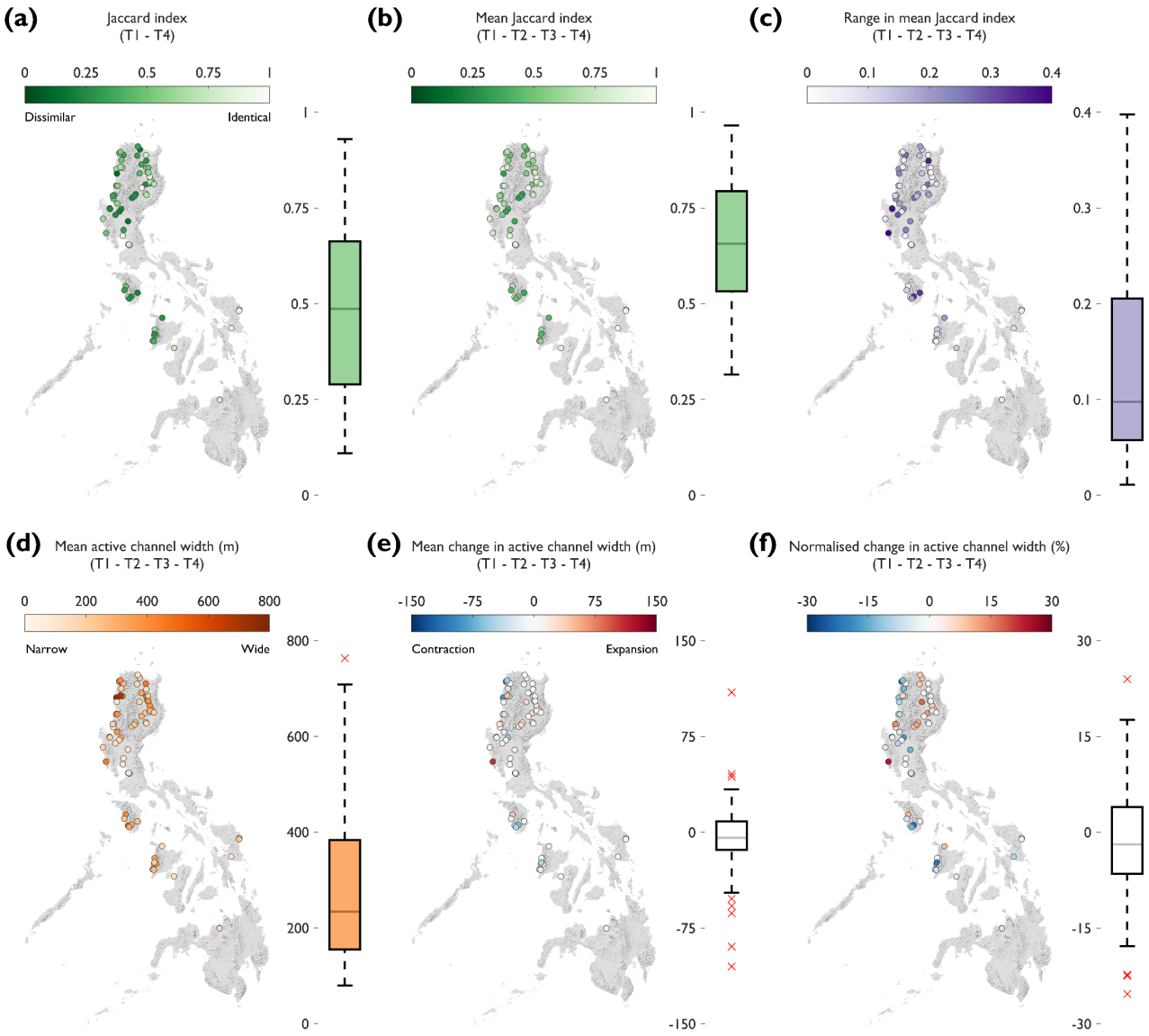


456

457 **Figure 6** – National-scale assessment of planform adjustment in the vicinity of large bridges. Planform
458 adjustment expressed by the distribution of Jaccard Index over engineering timescales (a); mean average
459 Jaccard Index over decadal timescales (b); and range in mean Jaccard index (c). Active channel width
460 expressed by the mean active channel width (d); mean change in active channel width (e); and normalised
461 change in active channel width (f).

462

462

463 **Table 3 –** Active channel width and temporal changes in the vicinity of critical bridge infrastructure (*n* = 74).
464 Active channel width metrics are calculated over decadal timescales (i.e. from T1 and T2, T2 and T3, T3 and
465 T4).

| | Metric | Time period | Mean | Median | SD | Min | Max | Range | 25th | 75th |
|---|---|---|---|---|---|---|---|---|---|---|
| Planimetric change | Jaccard index (T1 – T4) | T1 – T4 | 0.497 | 0.487 | 0.218 | 0.109 | 0.930 | 0.821 | 0.299 | 0.660 |
| | Mean Jaccard index | (T1 – T2 – T3 – T4) | 0.653 | 0.657 | 0.173 | 0.315 | 0.965 | 0.650 | 0.533 | 0.793 |
| | Range in mean Jaccard index | (T1 – T2 – T3 – T4) | 0.137 | 0.097 | 0.103 | 0.011 | 0.398 | 0.387 | 0.058 | 0.204 |
| Active channel width | Mean active channel width (m) | (T1 – T2 – T3 – T4) | 273.9 | 233.7 | 152.2 | 79.5 | 763.2 | 683.8 | 156.0 | 381.2 |
| | SD active channel width (m) | (T1 – T2 – T3 – T4) | 124.2 | 100.7 | 80.0 | 25.3 | 465.3 | 439.9 | 65.2 | 149.0 |
| | Mean active channel change (m) | (T1 – T2 – T3 – T4) | -4.7 | -4.4 | 30.0 | -105.2 | 109.5 | 214.7 | -13.4 | 8.6 |
| | Normalised change in mean active channel width (%) | (T1 – T2 – T3 – T4) | -1.5 | -1.9 | 9.1 | -25.3 | 24.0 | 49.3 | -6.3 | 3.7 |

466

467

468 Planform adjustments are plotted against the normalised change in active river channel width (Figure 7a
469 and b). In general, the maximum Jaccard index values at the extreme positive and negative values of
470 normalised change in active channel width are lower than the maximum values where there is little channel
471 width change. Based on the data, we define three indicative zones of active channel width behaviour:
472 negligible change where values fall within the 25$^{th}$ to 75$^{th}$ percentile of normalised change; channel
473 contraction where values are less than the 25$^{th}$ percentile; and channel expansion where values are greater

than the 75th percentile. All three behavioural zones are characterised by planform adjustment (including the negligible change zone), with considerable scatter throughout. The data indicate that planform adjustment is not limited to locations where there is a signal of channel contraction or expansion. Planform adjustment is also taking place at locations where the active channel width is maintained, so at these locations either: (i) the channel is shifting in position (i.e. migrating) but the planform geometry remains unchanged; or, (ii) localised channel expansion is approximately equal to channel contraction (i.e. a compensatory relationship between expansion and contraction). Conversely, for locations characterised by an overall signal of contraction or expansion behaviour, but the planform remains relatively stable (high Jaccard index), then a large active channel width could be dampening the overall planform response (i.e. the majority of the planform is not adjusting, but local width changes may be important). Results begin to indicate the diverse and complex planform adjustments at critical bridge infrastructure in the Philippines.

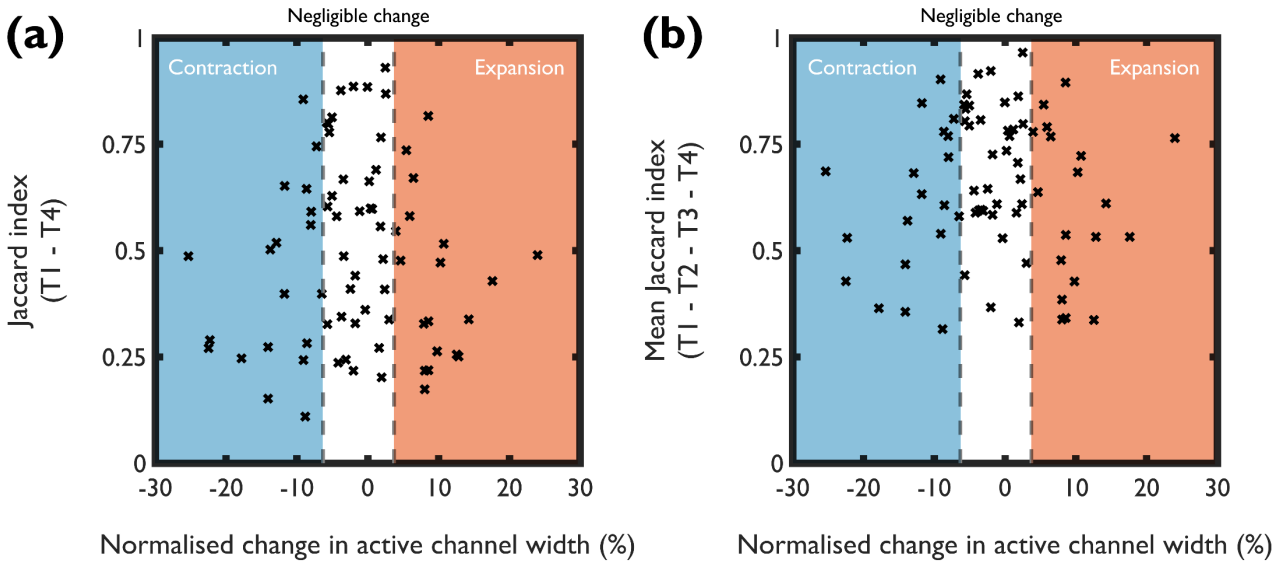


**Figure 7** – Planform change against normalised change in the active channel width for the Jaccard index (a) and the mean Jaccard index (b). Grey lines indicate the 25th and 75th percentile of normalised change in active channel width (Table 3). These values define geomorphic behavioural zones of negligible width change (white zone), channel contraction (blue zone) and channel expansion (red zone).

We observe no relationships between the built characteristics of bridges or stream network characteristics and planform adjustment over engineering timescales (Figure 8). Large bridges continue to be constructed at sites where planform adjustment has occurred (Figure 8a). This is not surprising, given that Philippine communities are often located proximal to river systems, with settlements in lowland areas likely better for agriculture, and population pressures driving the need for infrastructure development. Although bridges tend to be positioned closer to catchment outlets (Figure 5b), variation in planform adjustment is substantial across all positions along the stream network (Figure 8b). Proximal to channel outlets (normalised position along trunk stream > 0.75), the Jaccard index shows substantial variation and ranges between 0.11 to 0.88. Similarly, there appears to be no correlation between bridge length (Figure 8c) or catchment area (Figure 8d) and planform adjustment.

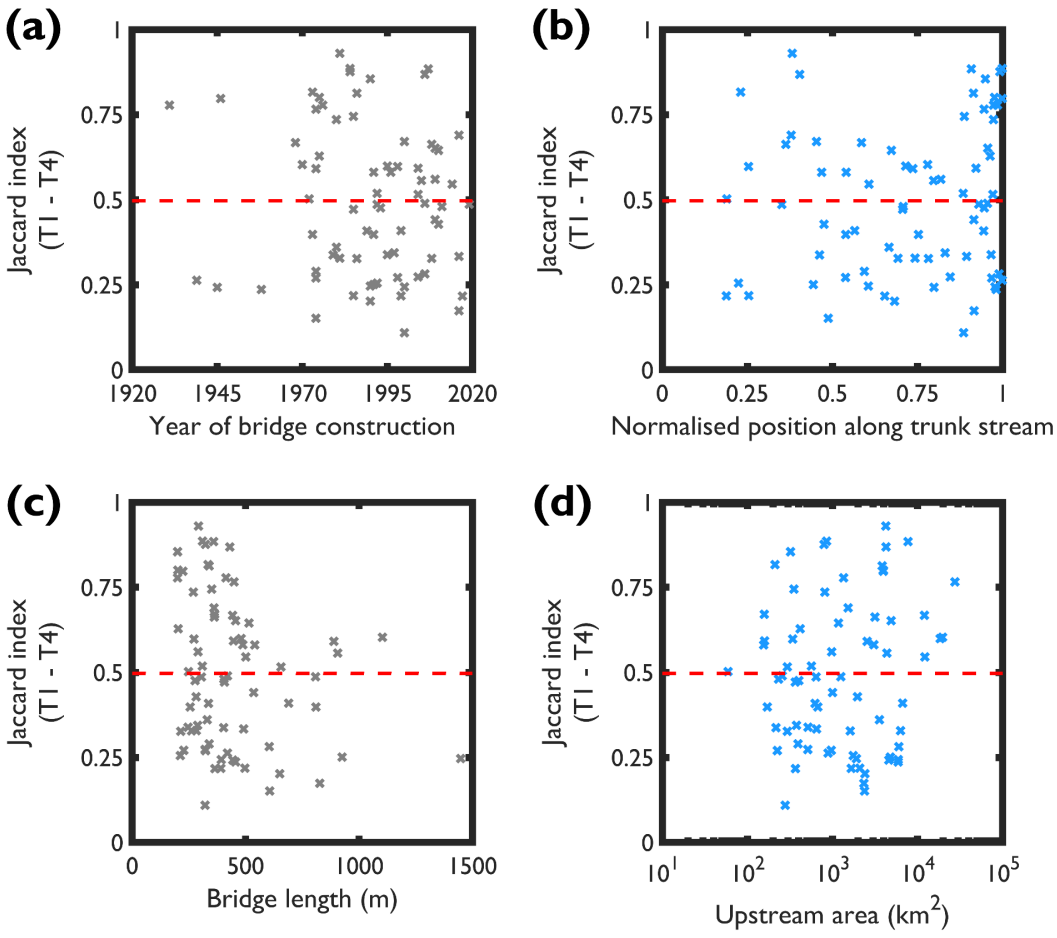

**Figure 8 –** Control of bridge characteristics and stream network configuration on planform adjustment over engineering timescales. Year of bridge construction (a); bridge position expressed as the normalised distance along the trunk stream (b); bridge length (c); and upstream area (d). Horizontal red dashed line indicates the mean Jaccard index = 0.497.

### 3.3. Geomorphic controls on planform adjustment

The local geomorphic setting (confinement, number of threads and channel pattern) imposes a fundamental control on the planform response at bridges (Figure 9). Bridges crossing confined rivers (Figure 9a and d) with straight channel patterns (Figure 9c and f) show less planform adjustment, narrower active channel widths and values of normalised change in active channel width closer to zero (i.e. negligible width changes though time). Bridges across partly-confined and laterally unconfined rivers show more planform adjustment (and greater variation in the amount of adjustment observed), active channel widths across the full data range and normalised change values over the full range of active channel behaviours (negligible change, contraction and expansion). On the number of threads (Figure 9b and e), rivers with multiple threads are characterised by wider active channels (mean active channel width for single thread = 221.4 m; multiple threads = 383.2 m) and slightly more planform adjustment (mean Jaccard index for single thread = 0.52; multiple threads = 0.44). A range of planform adjustment behaviour is observed across meandering, wandering and braided channel patterns (Figure 9c and f). Although planform adjustment is likely at all these sites, braided rivers show the greatest propensity to change. Together, the analyses begin to reveal the morphological diversity of rivers at bridge sites; an appreciation of the local geomorphic setting is essential for understanding the potential for river migration.

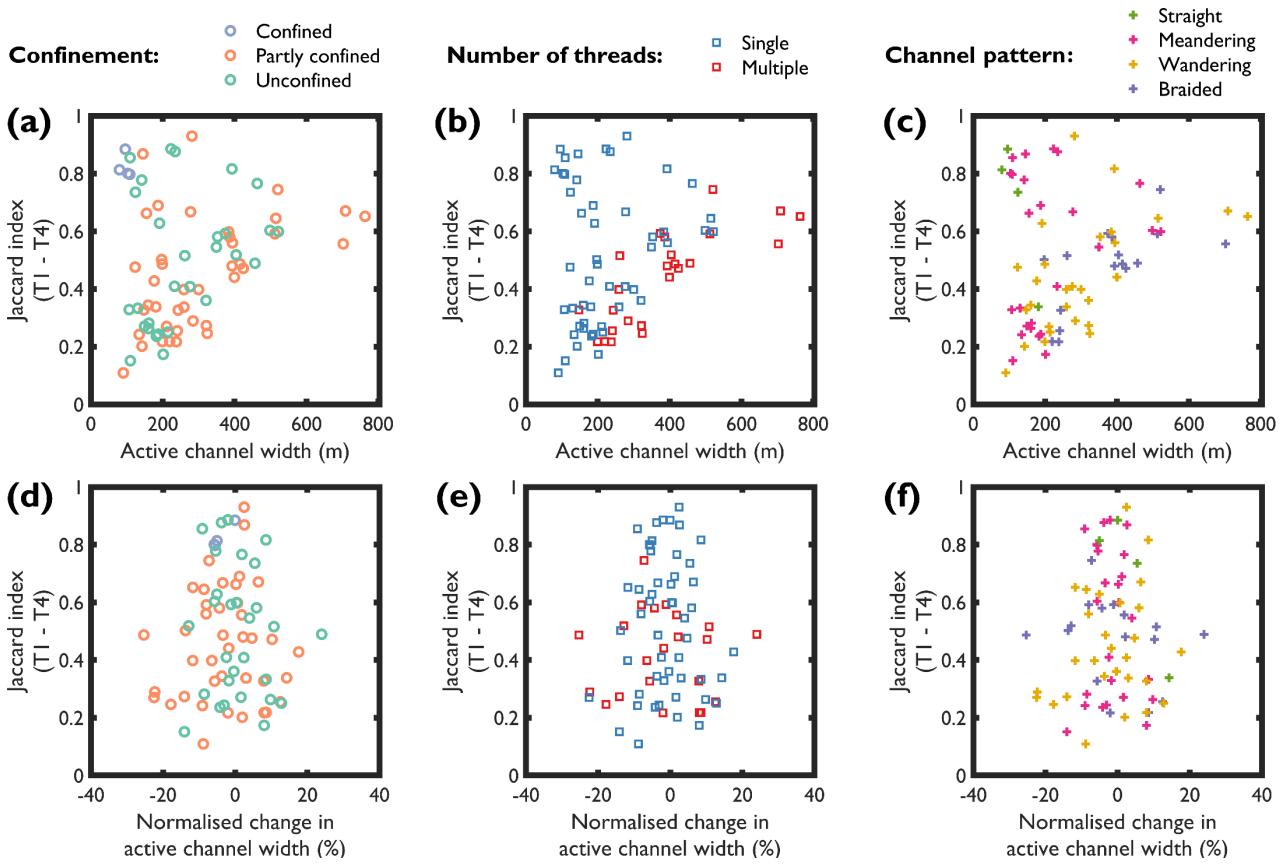


525

526 **Figure 9** – Geomorphic controls on planform adjustment (a-c) and normalised change in active channel
527 width (d-f). Data grouped by geomorphic setting including confinement, number of threads and channel
528 pattern.

529 For the indicative behaviours identified in Figure 7, we further investigate planform adjustments and active
530 channel width changes at three bridges (Figure 10). At the Bubulayan Bridge on the Abulug River (Apayao,
531 Luzon) marked planform adjustment (Jaccard index 0.33) resulted in overall channel expansion (Figure 10a).
532 For this partly-confined, multi-threaded wandering channel, the mean active channel width increased by
533 29% between 1988-89 and 2018-19, from 125 to 160 m ($n$ = 396 in T1, $n$ = 344 in T4). However, planform
534 adjustment and active channel expansion processes were spatially variable, with most of the adjustment
535 located downstream of the bridge. A transition in valley setting from confined to partly-confined could
536 partly explain the spatially variable patterns of river adjustment observed at the site. At the Jones Bridge on
537 the Cagayan River (Isabela, Luzon) planform adjustment was less marked (Jaccard index 0.66) with only
538 negligible change in active channel width (Figure 10b). For this unconfined, single-threaded meandering
539 channel, the mean active channel width increased by only 1% (162 to 163 m; $n$ = 647 in T1, $n$ = 627 in T4).

The distribution of active channel widths remained approximately unchanged over the engineering timescale and the planform was relatively stable. Inspection of contemporary, high-resolution satellite imagery in Google Earth showed discontinuous pockets of exposed bedrock in the reach and several river control structures (e.g. hard engineering defences) that potentially limit the capacity for river adjustment. At the Lumintao Bridge on the Lumintao River (Mindoro Occidental, Luzon) relatively minor planform adjustment through channel contraction was observed (Figure 10c). For this partly-confined, multi-threaded braided channel, the mean active channel width decreased by 19%, from 589 to 476 m ($n$ = 243 in T1; $n$ = 271 in T4). However, because the active channel area was initially large (5.96 $km^2$ in T1; 5.18 $km^2$ in T4) and width changes were highly localised, the Jaccard index remained high (Jaccard index 0.75). Colonisation of the inactive channel by riparian vegetation provides a possible explanation for the observed width changes, indicating the importance of biogeomorphic interactions on river evolution trajectory. Results exemplify that planform adjustments tend to be highly localised to specific parts of river reaches in the vicinity of critical bridge infrastructure, indicating the spatially heterogeneous nature of river migration and planform response.

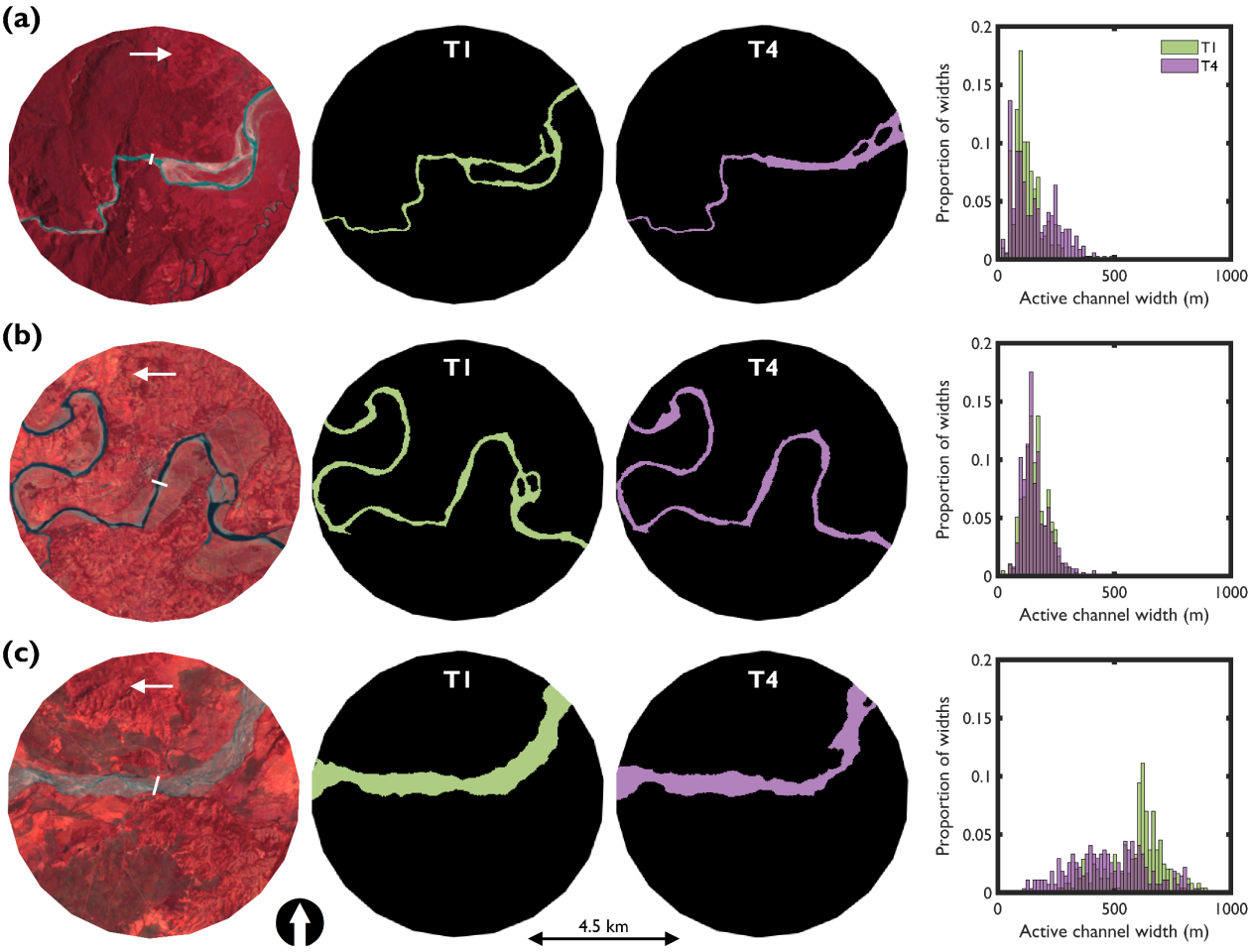


554

555 **Figure 10 –** Planform adjustments and width changes between 1988-89 (T1) and 2018-19 (T4) at the

556 Bubulayan Bridge (18°05'59.7"N 121°18'46.6"E), Abulug River (a); Jones Bridge (16°33'12.3"N

557 121°42'18.2"E), Cagayan River (b); and Lumintao Bridge (12°31'18.2"N 120°59'14.4"E), Lumintao River (c).

558 False colour composite from T1 shows bridge locations represented by white lines, white arrows denote

559 flow direction.

## 4. Discussion

### 4.1. Implications of river migration at critical bridge infrastructure in the Philippines

Multi-temporal analysis of multi-spectral satellite imagery has revealed the diversity of river planform adjustments in the vicinity of critical bridge infrastructure in the Philippines over decadal and engineering (30-year) timescales (e.g. Figures 6 and 7). Planform adjustment is substantial in the vicinity of some bridges, but for others the planform has remained approximately unchanged with only very limited changes in the active river channel width over three decades of analysis. Differences between bridge sites at the national-scale are partly explained by the significant geomorphic diversity exhibited by tropical rivers (Latrubesse et al., 2005; Sinha and Latrubesse, 2020). Crucially, different types of rivers adjust in different ways (Brierley and Fryirs, 2009), and this difference is being reflected in our national-scale results. In assessing geomorphic controls on planform adjustment and normalised change in channel width (Figure 9), fundamental differences in the characteristics and morphological behaviours emerge between bridges of different valley confinement settings and channel patterns (i.e. planform adjustment for a confined, single-threaded straight river differs from an unconfined, multi-threaded braided river). Further, we show the local and spatially heterogeneous nature of planform adjustment in the vicinity of bridge infrastructure (e.g. Figure 10a), with geomorphic processes not acting uniformly along the river reach. For unconfined rivers, active channel widening indicates bed aggradation, whereas narrowing indicates bed degradation or, on occasions, morphodynamic stabilisation by vegetation. As such, the manifestation of lateral adjustments cannot be separated from vertical adjustments at these sites. From a baseline, place-based understanding of river forms and processes, contextualized within the local catchment, we can begin to unravel the complexities of river migration at individual sites of critical bridge infrastructure. In doing so, it is critical to recognise the diversity, appraise the dynamics and understand the trajectory of each river system individually (Brierley and Fryirs, 2009).

Looking to the future, climate change is transforming the frequency and magnitude of typhoons and tropical storms, so increasing flooding and geomorphic risks, which may undermine the stability of bridges,

levees and other infrastructure (Eccles, 2019). In the Philippines, increases in the country-averaged median intensity of extreme rainfall have been observed in the period 1911-2010 (Villafuerte II et al., 2015) and future increases in river flow magnitude and variability are projected (Tolentino et al., 2016). Flood frequency and magnitude can have a significant effect on the scour performance of bridges (Imam, 2019) and the Chartered Institution of Water and Environmental Management (CIWEM) considers the risks posed by climate change to represent arguably the greatest long-term threat to critical infrastructure (ICE, 2009). However, it is unlikely that climate change impacts will be homogeneously expressed across the country; future projections from multiple dynamically downscaled climate model simulations suggest a tendency for wetter conditions to prevail over northern and central sections of the Philippines, particularly during the wet season (Villafuerte II et al., 2020). The projection for wetter conditions overlaps with the majority of large bridges in our inventory (Figure 6). We suggest that continued monitoring of planform adjustment will be essential for the long-term management of critical bridge infrastructure in the Philippines, particularly due to the projected impacts of climate change.

### 4.2. Additional factors that influence the relative risk at critical bridge infrastructure

River migration is not the only risk factor to critical bridge infrastructure in the Philippines. River adjustments are inherently three-dimensional and vertical adjustments can pose hazards through bed aggradation and scour (Lagasse et al., 2004). High sediment supply (e.g. from volcanic eruptions or typhoons) can cause localised bed aggradation that reduces the channel conveyance capacity, enhancing the effects of floods and increasing the potential for channel avulsion (Hayes et al., 2002). With the bedload flux from tropical catchments globally high (Syvitski et al., 2014), this could also contribute towards enhanced rates of general, local and contraction scour (Maddison, 2012). Significant planform changes associated with the propagation of sediment from the Assam earthquake in 1950 have been recorded in the vicinity of bridges on the Padma and Jamuna Rivers, Bangladesh, indicating that disturbance effects can be long-lived and that sediment flux can pose a legacy challenge (Sarker and Thorne, 2006). Similar sediment legacy effects (inputs from earthquakes and volcanic eruptions) are likely to be present in Philippine rivers (e.g. Mount Pinatubo; Gran and Montgomery, 2005). In addition to issues around sediment flux, accumulations of in-channel wood at bridges can pose local geomorphic hazards (Ruiz-Villanueva et

al., 2016; de Cicco et al., 2018; Panici et al., 2020). For comparable tropical catchments in Taiwan, significant volumes of wood enter fluvial systems during typhoon events (West et al., 2011), and tree debris are commonly entrained by mass wasting events in the Philippines (Rodolfo et al., 2016). Direct anthropogenic actions in rivers, including sand and gravel mining activities, pose further risks to riverbank stability (Bendixen et al., 2019; Hackney et al., 2020). Although it is recommended that extraction activities are carried out > 500 m from bridges to prevent excess aggradation or bridge pile scour in the Philippines (Vallejo, 2015), it is unclear whether this advice is strictly adhered to. Alterations to the natural flow regime (e.g. construction of hydropower dams) could further influence flood pulse dynamics and the floodplain geomorphology (Timpe and Kaplan, 2017). At the catchment-scale, changes in hydrology, land use and the removal of vegetation can further exacerbate river migration (Lagasse et al., 2004).

### 4.3. River migration at critical bridge infrastructure: placing findings from the Philippines into the global context

The causes of bridge failure in tropical river settings are not well documented. Literature analysis of 36 bridges failures from New Zealand, USA and Canada showed that scour accounted for 64% of bridge failures, while planform adjustment processes (specifically river migration) accounted for only 14% (Lin et al., 2014). For context, channel centreline normal migration rates for rivers in the USA range from 0.4 to 11% of the channel bankfull width per year (Melville and Coleman, 2000). Although we do not calculate channel migration rates directly, we demonstrate the planform dissimilarity over engineering timescales and report maximum active channel contraction and expansion equal to approximately 25% of channel width over decadal timescales (Table 2 and Figure 6 and 7). Combined with data from Dingle et al., (2019), who report channel migration rates > 300 m per decade at sites along the Cagayan River and the Pinacanauan de Ilagan (Luzon), the analyses begin to reveal the dynamic behaviour of some Philippine rivers. Where river migration rates are typically higher in tropical rivers than temperate rivers (Dingle et al., 2019), this will likely have implications for the relative importance of river migration as a failure mechanism at critical bridge infrastructure. However, in recognising the diversity of the morphological behaviours within our dataset, we note that not all sites exhibited pronounced river migration (e.g. Figure 10b). In the UK and many other, mainly temperate, regions, existing data allow assessments of potential future river

migration to be made, facilitating infrastructure risk assessment and planning (e.g. SEPA, 2010). Given the differences in river character, behaviour and evolution between temperate and tropical river settings, these protocols are unlikely to be readily transferable. Instead, site-specific understanding informed by knowledge of the local catchment (including hydrology, fluvial geomorphology and natural hazards) is essential in the effective planning, placement and management of critical bridge infrastructure, helping to mitigate potentially avoidable damages and failures (e.g. Figure 1). A concerted effort between national agencies and international bodies for the establishment of archival databases that accurately record bridge failure mechanisms would help to provide a global perspective on bridge failure. These could potentially build on previous attempts to record global bridge failure incidence (e.g. the Bridge Collapse Database that was operational until 2009; Imhof and Middleton, 2010).

### 4.4. Methodological uncertainties

Several uncertainties in the current application are acknowledged. Differing edge representations between the ground truth (vector) and classified (raster) datasets could introduce small areal discrepancies into the initial accuracy assessments (Table 1). Temporal compositing produced 'average' representations of the active river channel; with planform adjustments identified over decadal timescales. Although the analyses reveal gross adjustment in river planform over decadal/engineering timescales, they mask the compensatory changes in the intervening period (Boruah et al., 2008; Kondolf and Piégay, 2016), so provide only multiple snapshots of river evolution rather than a continuous record. Analyses should continue to be applied at timescales relevant to the functional timescales of geomorphic processes of interest (Boothroyd et al., 2020) and here it is important to comment on what might be missing from the satellite imagery data archive. Although available satellite imagery data archives may extend back to the 1970s, the natural relaxation time after disturbance for large river systems is likely to be significantly longer than that of the data available (Church, 1996).

A key source of uncertainty was introduced during the delineation of the active river channel. Although the accuracy assessment showed that more than 80% of the active channel was correctly identified through our GEE workflow, the classification provides a conservative underprediction of the active channel extent

(particularly when omitting active channel boundary edge regions). Where satellite imagery pixel edges do not coincide with the edges of objects on the ground, pixels contain several objects (e.g. bed material, water and vegetation; Gilvear and Bryant, 2016). Even for the largest rivers, mixed pixels are found at the boundaries between bank lines and channel bar boundaries (Gupta et al., 2013). Further, the accuracy of boundary delineation is influenced by channel width and morphological complexity. Narrow channels, particularly those with variations in riparian vegetation abundance and highly complex bar arrangements, are associated with greater bankline delineation errors (Rowland et al., 2016; Werbylo et al., 2017; Donovan et al., 2019). To minimise these effects, we restricted our analysis to large bridges (> 200 m wide). To further address these issues, a comprehensive framework for evaluating uncertainty in estimates of river migration and channel width changes could be applied (e.g. Donovan et al., (2019)). Such frameworks encourage the use of spatially variable level of detection (LoD) thresholds to determine statistically significant changes in river planform, helping account for the multitude of error sources in bankline delineation.

Recent and future improvements in the spatial resolution of satellite imagery will further increase the applicability of similar approaches to smaller river systems (Khorram et al., 2016). Opportunities exist to leverage higher resolution Sentinel-2 satellite imagery (10 m spatial resolution). Likewise, even higher resolution optical satellite imagery (e.g. Airbus Pléiades, Maxar, PlanetScope) may reveal ever finer planform adjustments. Whilst these higher resolution records have limited archive length for historical analysis, they have value in the quantification of contemporary planimetric change. Here, analysis was limited to only include rivers where the active channel width exceeded 150 m (Section 2.1.1), so limited the number of bridge sites over which river migration could be assessed. As the record length increases for higher resolution satellite imagery, the approach becomes more feasible for narrower rivers. Regardless of pixel resolution, the classification of exposed fluvial sediment remains a challenge. Established multi-spectral indices exist for the classification of water (e.g. Zou et al., 2018) but the performance of these indices varies with background conditions (e.g. Rokni et al., 2014) and alternative water classification approaches could be incorporated into the GEE workflow (e.g. the Automated Water Extraction Index, AWEI; Feyisa et al., 2014). In contrast, comparable indices for the classification of exposed fluvial sediment

693 are yet to be fully developed and realised. Proof of concept work has been undertaken for small alluvial
694 reaches (e.g. Spada et al., 2018), but these are yet to be applied universally (i.e. between different river
695 systems) or at scale (i.e. at the catchment-scale). Parameters used to classify the active river channel in the
696 current application may not translate across a geodiverse range of settings (e.g. to different hydro-climatic
697 regions). The integration of optical remote sensing with high-spatial resolution sensors, ground-truth, and
698 *in situ* data could improve future accuracy assessment (Nguyen et al., 2019), but the research challenge
699 around the classification of exposed sediment remains.

700 **4.5. Implications for management**

701 Geomorphic risk at critical bridge infrastructure is commonly managed through assessment, monitoring
702 and maintenance protocols (Lamb et al., 2017), with risk-based approaches to bridge management formed
703 around the methodological framework elements of hazard, exposure and vulnerability (Pregnolato, 2019).
704 From an engineering perspective, specific frameworks have been developed to assess river channel stability
705 in the vicinity of bridges and culverts, including analyses of river bank processes (slope, failure modes,
706 material), vegetation and historic channel migration (e.g. HEC-20, Lagasse et al., 2012); point-based scoring
707 of geomorphic characteristics (e.g. Simon and Downs, 1995); quantitative assessment of hydraulic
708 geometries (e.g. Thorne et al., 1996); rapid assessment of weight-assigned stability indicators (e.g. Johnson
709 et al., 1999); and the characterisation of channels in different physiographic settings (e.g. Johnson, 2005). In
710 these frameworks a mixture of qualitative and quantitative stability indicators provide the overall
711 assessment of channel stability (Johnson et al., 1999). However, here we show that river migration is not a
712 local condition; it may extend beyond the vicinity of critical infrastructure, so may not be adequately
713 captured during local bridge inspections (Johnson and Whittington, 2011).

714 In designing bridge vulnerability assessment protocols and risk-based analysis models, Lamb et al., (2017)
715 recommend for the incorporation of hydraulic and morphologic change factors beyond the local site. This
716 extended view is more commonly practiced in assessments of river stability from a fluvial geomorphology
717 perspective, assessed at scales ranging from short river modules (e.g. the MoRPh framework; Shuker et al.,
718 2017) through to entire river catchments (e.g. the River Styles Framework: Brierley and Fryirs, 2005; fluvial

719 audit method: Sear et al., 2009). Knowledge of the catchment (including what is happening both upstream
720 and downstream of a particular site) is essential for contextualising the local adjustments (Brierley and
721 Fryirs, 2009), especially as disturbances may occur at any time and anywhere in a catchment (Gurnell et al.,
722 2015).

723 Satellite remote sensing provides an opportunity to monitor and provide a baseline understanding of
724 planimetric river adjustment in the vicinity of critical bridge infrastructure, but in isolation these data
725 should not be used to predict or estimate future trends. Reach- and catchment-scale factors influence river
726 adjustment, with complexity and uncertainty introduced by future climate change impacts (see Section 4.1.
727 and 4.2.). Understanding the spatiotemporal variability in river adjustment can provide a means of
728 determining what controls the nature of adjustment or change (Lisenby and Fryirs, 2016). However,
729 detailed appraisal of the geomorphology within the local catchment context is first needed (e.g. through
730 application of the River Styles Framework to understand river character and behaviour; Brierley and Fryirs,
731 2005). Then, different forms of river adjustment can be linked to hydrologic and morphometric variables
732 (e.g. unit stream power, Joyce et al., 2020; valley confinement, Khan and Fryirs; 2020) to develop spatially
733 distributed process domains or typologies of river adjustment (Lisenby and Fryirs, 2016). Here it is
734 important to recognise the local and spatially heterogeneous nature of river adjustment, meaning that a
735 single predictive equation for river adjustment is unlikely to be realised. Rather, monitoring and
736 geomorphic interpretation can contribute towards scenario-building exercises that forecast possibilities of
737 river adjustment and inform future river management decisions (Lisenby and Fryirs, 2020).

738 Monitoring can complement numerical modelling in providing independent calibration, verification and
739 validation data sets for the spatiotemporal analysis of river evolution. Hydraulic and morphodynamic
740 modelling is often performed in the vicinity of critical bridge infrastructure, including for flood-risk
741 assessment, sediment transport analysis and simulating the performance of river training measures (e.g.
742 McLean et al., 2012; Vasquez et al., 2012; Nones et al., 2018; Trueheart et al., 2020). From a
743 morphodynamic perspective, model calibration, verification and validation represents an ongoing research
744 challenge, especially for dynamic wandering and braided river systems; where topographic monitoring
745 techniques provide only a snapshot of morphological evolution and repeat survey data are infrequently

746 commensurate with the rates of morphological change (Williams et al., 2016). Satellite remote sensing
747 provides an opportunity to monitor abrupt and gradual changes in river planform owing to the higher
748 temporal revisit times of the sensors (e.g. with the increasing availability of sub-weekly and sub-daily
749 satellite imagery). However, rivers also adjust in the vertical dimension. These changes will not be captured
750 by two-dimensional planform analyses alone (Boothroyd et al., 2020) and are typically too small in their
751 vertical magnitude to be resolved from photogrammetric analysis of even the highest resolution satellite
752 imagery (Shean et al., 2016). An appreciation of these limitations is necessary when seeking to calibrate or
753 validate numerical models with data derived from satellite remote sensing, with the need to recognise the
754 uncertainties associated with the independent data sets and model outputs (Hoey et al., 2003).

755 We recommend the potential of multi-temporal analysis from satellite remote sensing as a low-cost
756 approach for monitoring planform adjustment and the relative risk of river migration at critical bridge
757 infrastructure (e.g. to support current DPWH activities). This low-cost approach could be performed as part
758 of large bridge vulnerability assessment and integrated with other Earth observation data to effectively
759 assess critical urban assets and infrastructure most at risk from flooding (Asian Development Bank, 2017).
760 Site-specific information from remotely sensed data (e.g. multi-temporal satellite imagery, topographic
761 analyses) can be readily appended to existing bridge geodatabases to help identify those sites most at risk.
762 Bridge specific assessments can then be performed using a 'minimal data' approach for higher resolution
763 data capture and assessment (e.g. Maniatis et al., 2019). Where necessary, direct measurement of
764 riverbank stability through topographic monitoring (e.g. using Terrestrial Laser Scanning, Williams et al.,
765 2015; airborne LiDAR, Nelson and Dubé, 2015; or structure-from-motion photogrammetry, Ozcan and
766 Ozcan, 2019) can quantify high resolution geomorphic change to further inform the management response.

767 We recommend that all results be contextualised within the local catchment, recognising the diversity,
768 appraising the dynamics and understanding the trajectory of each particular river system (Brierley and
769 Fryirs, 2009). We suggest that our remote sensing monitoring approach could help inform the strategic
770 planning and placement of critical bridge infrastructure but could also be applied more widely to other
771 forms of critical infrastructure adjacent to rivers (e.g. roads and rail). The approach and recommendations
772 could be extended beyond the Philippines to other dynamic riverine settings where river migration poses a

773 risk to critical infrastructure.

## 5. Conclusions

Multi-temporal satellite imagery analyses over three decades show that planform adjustment is widespread at sites of critical bridge infrastructure in the Philippines, with lateral channel adjustment (channel migration, contraction and expansion) recorded in the vicinity of large bridges (bridge deck length > 200 m). Using the Jaccard index to indicate planform (dis)similarity, the mean Jaccard index (0.50) indicates considerable planform adjustment at the 74 inventoried bridge sites over engineering timescales (50% of values in the range 0.30 to 0.66). The national-scale assessment reveals the diversity of planform adjustment at bridge sites on Philippine rivers (Figure 6). Some inventoried bridges are characterised by substantial planform adjustment and river migration, with maximum active channel contraction and expansion over decadal timescales equal to approximately 25% of the active channel width. This represents considerable lateral adjustment and when left unmanaged could pose a substantial geomorphic hazard to critical bridge infrastructure. However, for other inventoried bridges the planform has remained approximately unchanged. The local geomorphic setting is shown to impose a fundamental control on the planform adjustments observed, with different confinement settings and channel patterns characterised by different channel characteristics (e.g. active channel widths) and morphological behaviours. Results from individual bridges demonstrate the local and spatially heterogeneous nature of planform adjustment in the vicinity of large bridges (e.g. Figure 10). In understanding planform adjustments, it remains critical to recognise the diversity, appraise the dynamics and understand the trajectory of each river system individually (Brierley and Fryirs, 2009). This is particularly important for tropical rivers, where migration rates are typically higher than for temperate rivers (Dingle et al., 2019), and has implications for the relative importance of river migration as a failure mechanism at critical bridge infrastructure.

From a management perspective, our Google Earth Engine (GEE) workflow provides a useful tool for the spatiotemporal quantification of river planform adjustment. With access to big geospatial data (e.g. Landsat satellite imagery over engineering timescales) and higher resolution data for contemporary timescales, we recommend multi-temporal analyses as a low-cost approach for monitoring planform adjustment and the

relative risk of river migration at critical bridge infrastructure. Analyses could be formally incorporated into bridge monitoring investigations (e.g. as a component of bridge stability assessments) and used to inform the strategic design and placement of future bridge infrastructure. Moreover, approaches could be applied more widely to other forms of infrastructure adjacent to rivers (e.g. roads, rail, pipelines) and extended beyond the Philippines to other dynamic riverine settings where river migration poses a risk to critical infrastructure.

## Data availability

Google Earth Engine code to assess active river channel change (i.e. planform adjustment) is available here: https://code.earthengine.google.com/8ae6ae8a2c55eefbafa552216ff4c479.

The data set containing the Philippines bridge inventory and river migration geodatabase is available as part of the supplementary materials.

The Google Earth Engine code and Philippines bridge inventory and river migration geodatabase will be uploaded to the NERC Environmental Information Data Centre (EIDC) along with supporting documentation to enable continued open access to the data.

## Acknowledgements

We are grateful to the Philippines Department of Public Works and Highways (DPWH) for making bridge inventory data publicly available through the Detailed Bridge Inventory Application (https://dpwh.maps.arcgis.com/apps/webappviewer/index.html?id=1153f9b8f2324ad08b22f70a72432100 ). Data in the bridge inventory were provided by the Philippines Statistics Division, Planning Service and Department of Public Works and Highways. This research was undertaken as part of a Natural Environment Research Council (NERC) and Department of Science and Technology - Philippine Council for Industry, Energy and Emerging Technology Research and Development (DOST-PCIEERD) – Newton Fund grant (NE/S003312). We are grateful to the Associate Editor and two anonymous reviewers for providing helpful comments that led to significant improvements in this manuscript.

## Author contributions following CRediT

**Richard Boothroyd:** conceptualisation, investigation, methodology, visualisation, writing-original draft, writing-review and editing. **Richard Williams:** funding acquisition, project administration, writing-review

and editing. **Trevor Hoey:** funding acquisition, writing-review and editing. **Pamela Tolentino:** writing-review and editing. **Xiao Yang:** software, writing-review and editing.

## References


Arneson, L.A., Zevenbergen, L.W., Lagasse, P.F. and Clopper, P.E. 2012. Evaluating scour at bridges. Hydr. Eng. Circular No. 18: FHWA-HIF-12-003, U.S Department of Transportation. https://www.fhwa.dot.gov/engineering/hydraulics/pubs/hif12003.pdf

Aronica, G.T., Bates, P.D. and Horritt, M.S. 2002. Assessing the uncertainty in distributed model predictions using observed binary pattern information within GLUE. Hydrological Processes. 16(10), pp. 2001-2016. https://doi.org/10.1002/hyp.398

Asian Development Bank. 2017. Earth Observation for a Transforming Asia and Pacific. Asian Development Bank. https://www.adb.org/sites/default/files/publication/231486/earth-observation-asia-pacific.pdf

Baki, A.B.M. and Gan, T.Y. 2012. Riverbank migration and island dynamics of the braided Jamuna River of the Ganges–Brahmaputra basin using multi-temporal Landsat images. Quaternary International. 263, pp. 148-161. https://doi.org/10.1016/j.quaint.2012.03.016

Beechie, T.J., Liermann, M., Pollock, M.M., Baker, S. and Davies, J. 2006. Channel pattern and river-floodplain dynamics in forested mountain river systems. Geomorphology. 78(1-2), pp. 124-141. https://doi.org/10.1016/j.geomorph.2006.01.030

Bendixen, M., Best, J., Hackney, C. and Iversen, L.L. 2019. Time is running out for sand. Nature. 571 (7763), pp. 29-31. https://doi.org/10.1038/d41586-019-02042-4

Bertoldi, W., Drake, N.A. and Gurnell, A.M. 2011. Interactions between river flows and colonizing vegetation on a braided river: exploring spatial and temporal dynamics in riparian vegetation cover using satellite data. Earth Surface Processes and Landforms. 36(11), pp. 1474-1486. https://doi.org/10.1002/esp.2166

854 Best, J.L., Ashworth, P.J., Sarker, M.H. and Roden, J.E. 2007. The Brahmaputra-Jamuna River, Bangladesh.
855 Chapter 19 in A. Gupta (Ed.), Large Rivers: Geomorphology and Management, pp. 395-430. John Wiley &
856 Sons. https://doi.org/10.1002/9780470723722.ch19

857 Boothroyd, R.J., Williams R.D., Hoey, T., Barrett, B. and Prasojo, O.A. in press. Applications of Google Earth
858 Engine in fluvial geomorphology for detecting river channel change. *WIREs Water*.

859 Boruah, S., Gilvear, D., Hunter, P. and Sharma, N. 2008. Quantifying channel planform and physical habitat
860 dynamics on a large braided river using satellite data—the Brahmaputra, India. River Research and
861 Applications. 24(5), pp. 650-660. https://doi.org/10.1002/rra.1132

862 Boyce, R.L. and Ellison, P.C. 2001. Choosing the best similarity index when performing fuzzy set ordination
863 on binary data. Journal of Vegetation Science. 12(5), pp. 711-720. https://doi.org/10.2307/3236912

864 Briaud, J.L., Gardoni, P. and Yao, C. 2014. Statistical, risk, and reliability analyses of bridge scour. Journal of
865 Geotechnical and Geoenvironmental Engineering. 140(2), pp. 04013011.
866 https://doi.org/10.1061/(ASCE)GT.1943-5606.0000989

867 Brierley, G. and Fryirs, K.A. 2009. Don't Fight the Site: Three Geomorphic Considerations in Catchment-
868 Scale River Rehabilitation Planning. Environmental Management. 43, pp. 1201-1218.
869 https://doi.org/10.1007/s00267-008-9266-4

870 Brierley, G.J. and Fryirs, K.A. 2005. Geomorphology and River Management: Applications of the River Styles
871 Framework. Blackwell Publications.

872 Catane, S.G., Abon, C.C., Saturay Jr, R.M., Mendoza, E.P.P. and Futalan, K.M. 2012. Landslide-amplified flash
873 floods—the June 2008 Panay Island flooding, Philippines. Geomorphology, 169, pp. 55-63.
874 https://doi.org/10.1016/j.geomorph.2012.04.008

875 Choi, S.S., Cha, S.H. and Tappert, C.C. 2010. A survey of binary similarity and distance measures. Journal of
876 Systemics, Cybernetics and Informatics. 8(1), pp. 43-48.

877 Church, M. 1996. Space, time and the mountain – how do we order what we see? In B. L. Rhoads and T. C.E
878 (Eds.), The Scientific Nature of Geomorphology: Proceedings of the 27th Binghamton Symposium in
879 Geomorphology (pp. 147-170).

880 Church, M. 2006. Bed material transport and the morphology of alluvial river channels. Annual Review of
881 Earth Planet Sciences. 34, pp. 325-354. https://doi.org/10.1146/annurev.earth.33.092203.122721

882 Clifford, H.T. and Stephenson, W. 1975. An introduction to numerical classification. Academic Press.

883 Coleman, S.E. and Melville, B.W. 2001. Case study: New Zealand bridge scour experiences. Journal of
884 Hydraulic Engineering. 127(7), pp. 535-546. https://doi.org/10.1061/(ASCE)0733-9429(2001)127:7(535)

885 Cotton, J.K. 1999. Effect of geomorphic hazards on bridge reliability. In Richardson, E.V. and Lagasse, P.F.
886 (Eds), Stream stability and scour at highway bridges. pp.129-144. ASCE Publications.

887 De Cicco, P.N., Paris, E., Ruiz-Villanueva, V., Solari, L. and Stoffel, M. 2018. In-channel wood-related hazards
888 at bridges: A review. River Research Applications. 34, pp. 617-628. https://doi.org/10.1002/rra.3300

889 Department of Public Works and Highways (DPWH). 2018. Strengthening economic resilience and spurring
890 infrastructure growth. 25 September 2018. London: United Kingdom.
891 https://iro.ph/article_doc/82a590ff_Philippine%20Infrastructure%20-
892 %20Latest%20Developments%20in%20Roads%20and%20Highway%20Sector%20(DPWH).pdf

893 Department of Public Works and Highways (DPWH). 2020. Detailed Bridge Inventory Application. Available
894 online at:
895 https://dpwh.maps.arcgis.com/apps/webappviewer/index.html?id=1153f9b8f2324ad08b22f70a72432100

896 Department of Public Works and Highways (DPWH) Regional Office II. 2020. Final Annual Procurement Plan
897 for FY 2018. Available online at: https://www.gppb.gov.ph/gppb-admin/monitoring/app/APP2018_DPWH-
898 ROII.pdf

899 Donovan, M., Belmont, P., Notebaert, B., Coombs, T., Larson, P. and Souffront, M. 2019. Accounting for
900 uncertainty in remotely-sensed measurements of river planform change. Earth-Science Reviews. 193, pp.
901 220-236. https://doi.org/10.1016/j.earscirev.2019.04.009

902 Dice, L.R. 1945. Measures of the amount of ecologic association between species. Ecology. 26, pp. 297-302.

903 Dingle, E.H., Paringit, E.C., Tolentino, P.L.M., Williams, R.D., Hoey, T.B., Barrett, B., Long, H., Smiley, C. and
904 Stott, E. 2019. Decadal-scale morphological adjustment of a lowland tropical river. Geomorphology. 333,
905 pp. 30-42. https://doi.org/10.1016/j.geomorph.2019.01.022

906 Eccles, R., Zhang, H. and Hamilton, D. 2019. A review of the effects of climate change on riverine flooding in
907 subtropical and tropical regions. Journal of Water and Climate Change. 10, pp. 687-707.
908 https://doi.org/10.2166/wcc.2019.175

909 Enke D.L., Tirasirichai, C. and Luna, R. 2008. Estimation of earthquake loss due to bridge damage in the St.
910 Louis metropolitan area. II: Indirect losses. Natural Hazard Reviews. 9, pp. 12-9.
911 https://doi.org/10.1061/(ASCE)1527-6988(2008)9:1(12)

912 Feyisa, G.L., Meilby, H., Fensholt, R. and Proud, S.R. 2014. Automated Water Extraction Index: A new
913 technique for surface water mapping using Landsat imagery. Remote Sensing of Environment. 140, pp. 23-
914 35. https://doi.org/10.1016/j.rse.2013.08.029

915 Foga, S., Scaramuzza, P.L., Guo, S., Zhu, Z., Dilley, R.D., Beckmann, T., Schmidt, G.L., Dwyer, J.L., Hughes,
916 M.J. and Laue, B. 2017. Cloud detection algorithm comparison and validation for operational Landsat data
917 products. Remote Sensing of Environment. 194, pp. 379-390. https://doi.org/10.1016/j.rse.2017.03.026

918 Fryirs, K.A. 2017. River sensitivity: a lost foundation concept in fluvial geomorphology. Earth Surface
919 Processes and Landforms. 42(1). pp. 55-70. https://doi.org/10.1002/esp.3940

920 Gilvear, D.J. and Bryant, R. 2016. Analysis of remotely sensed data for fluvial geomorphology and river
921 science. In Kondolf, M. and Piégay, H. (Eds.), Tools in Fluvial Geomorphology. (pp. 103-132).
922 https://doi.org/10.1002/9781118648551.ch6

923 Gob, F., Gautier, E., Virmoux, C., Grancher, D., Tamisier, V., Primanda, K.W., Wibowo, S.B., Sarrazin, C., de
924 Belizal, E., Ville, A. and Lavigne, F. 2016. River responses to the 2010 major eruption of the Merapi volcano,
925 central Java, Indonesia. Geomorphology. 273, pp. 244-257.
926 https://doi.org/10.1016/j.geomorph.2016.08.025

927 Gorelick, N., Hancher, M., Dixon, M., Ilyushchenko, S., Thau, D. and Moore, R. 2017. Google Earth Engine:
928 Planetary-scale geospatial analysis for everyone. Remote Sensing of Environment. 202, pp. 18-27.
929 https://doi.org/10.1016/j.rse.2017.06.031

930 Grabowski, R.C., Surian, N. and Gurnell, A.M. 2014. Characterizing geomorphological change to support
931 sustainable river restoration and management. WIREs Water. 1(5), pp. 483-512.
932 https://doi.org/10.1002/wat2.1037

933 Grafil, L. and Castro, O. 2014. Acquisition of IfSAR for the Production of Nationwide DEM and ORI for the
934 Philippines under the Unified Mapping Project. Infomapper, 21, pp. 12-13 and 40-43.

935 Gran, K.B. and Montgomery, D.R. 2005. Spatial and temporal patterns in fluvial recovery following volcanic
936 eruptions: Channel response to basin-wide sediment loading at Mount Pinatubo, Philippines. GSA Bulletin.
937 117(1-2), pp. 195-211. https://doi.org/10.1130/B25528.1

938 Gran, K.B., Montgomery, D.R. and Halbur, J.C. 2011. Long-term elevated post-eruption sedimentation at
939 Mount Pinatubo, Philippines. Geology. 39(4), pp. 367-370. https://doi.org/10.1130/G31682.1

940 Gupta, N., Atkinson, P. M. and Carling, P.A. 2013. Decadal length changes in the fluvial planform of the
941 River Ganga: bringing a mega-river to life with Landsat archives. Remote Sensing Letters. 4(1), pp. 1-9.
942 https://doi.org/10.1080/2150704X.2012.682658

943 Gurnell, A.M., Rinaldi, M., Belletti, B., Bizzi, S., Blamauer, B., Braca, G., Buijse, A.D., Bussettini, M., Camenen,
944 B., Comiti, F., Demarchi, L., García de Jalón, D., González del Tánago, M., Grabowski, R.C., Gunn, D.M.,
945 Habersack, H., Hendriks, D., Henshaw, A.J., Klösch, M., Lastoria, B., Latapie, A., Marcinkowski, P., Martínez-
946 Fernández, V., Mosselman, E., Mountford, J.O., Nardi, L., Okruszko, T., O'Hare, M.T., Palma, M., Percopo,
947 C., Surian, N., van de Bund, W., Weissteiner, C. and Ziliani, L. 2015. A multi-scale hierarchical framework for

948 developing understanding of river behaviour to support river management. Aquatic Sciences. 78, pp. 1-16.
949 https://doi.org/10.1007/s00027-015-0424-5

950 Hackney, C.R., Darby, S.E., Parsons, D.R., Leyland, J., Best, J.L., Aalto, R., Nicholas, A.P. and Houseago, R.C.
951 2020. River bank instability from unsustainable sand mining in the lower Mekong River. Nature
952 Sustainability. 3, pp. 217-225. https://doi.org/10.1038/s41893-019-0455-3

953 Haralick, R.M., Sternberg S.R. and Zhuang, X. 1987. Image Analysis Using Mathematical Morphology. IEEE
954 Transactions on Pattern Analysis and Machine Intelligence. 9(4), pp. 532-550.
955 https://doi.org/10.1109/TPAMI.1987.4767941

956 Hayes, S.K., Montgomery, D.R. and Newhall, C.G. 2002. Fluvial sediment transport and deposition following
957 the 1991 eruption of Mount Pinatubo. Geomorphology. 45(3-4), pp. 211-224.
958 https://doi.org/10.1016/S0169-555X(01)00155-6

959 Hoey, T.B., Bishop, P. and Ferguson, R.I. 2003. Testing Numerical Models in Geomorphology: How can we
960 Ensure Critical Use of Model Predictions?. In Prediction in Geomorphology (eds) P.R. Wilcock and R.M.
961 Iverson. https://doi.org/10.1029/135GM17

962 Hohn, M.E., 1976. Binary coefficients: A theoretical and empirical study. Journal of the International
963 Association for Mathematical Geology, 8(2), pp. 137-150. https://doi.org/10.1007/BF01079031

964 Horritt, M.S. and Bates, P.D. 2001. Predicting floodplain inundation: raster-based modelling versus the
965 finite element approach. Hydrological Processes. 15(5), pp. 825-842. https://doi.org/10.1002/hyp.188

966 Huete, A., Didan, K., Miura, T., Rodriguez, E.P., Gao, X. and Ferreira, L.G. 2002. Overview of the radiometric
967 and biophysical performance of the MODIS vegetation indices. Remote Sensing of Environment. 83(1), pp.
968 195-213. https://doi.org/10.1016/S0034-4257(02)00096-2

969 Imam, B., 2019. Climate change impact for bridges subjected to scour and corrosion. In Bastidas-Arteaga, E.
970 and Stewar, M.G. (Eds), Climate Adaptation Engineering (pp. 165-206). Butterworth-Heinemann.
971 https://doi.org/10.1016/B978-0-12-816782-3.00006-1

Imhof, D. and Middleton, C. 2010. Bridge Collapse Database. Available online at: https://www.bridgeforum.org/dir/collapse/

Institution of Civil Engineers (ICE). 2009. The State of the Nation: Defending Critical bridge infrastructure. Institute of Civil Engineers. https://www.ice.org.uk/getattachment/media-and-policy/policy/state-of-the-nation-critical-infrastructure-2009/SoN_DCIreport_final_web.pdf.aspx

Islam, R., Islam, M.N. and Islam, M.N., 2017. Impacts of Bangabandhu Jamuna multi-purpose bridge on the dynamics of bar morphology at the Jamuna River in Bangladesh. Modeling Earth Systems and Environment. 3(3), pp. 903-925. https://doi.org/10.1007/s40808-017-0342-8

Jaccard, P. 1901. Distribution de la flore alpine dans le Bassin des Dranses et dans quelques regions voisines. Bulletin de la Societ´ e Vaudoise des Sciences Naturelles, 37, pp. 241-272.

Johnson, P.A. and Whittington, R.M. 2011. Vulnerability-based risk assessment for stream instability at bridges. Journal of Hydraulic Engineering. 137(10), pp. 1248-1256. https://doi.org/10.1061/(ASCE)HY.1943-7900.0000443

Johnson, P.A. 2005. Preliminary assessment and rating of stream channel stability near bridges. Journal of Hydraulic Engineering. 131(10), pp. 845-852. https://doi.org/10.1061/(ASCE)0733-9429(2005)131:10(845)

Johnson, P.A., Gleason, G.L. and Hey, R.D. 1999. Rapid assessment of channel stability in vicinity of road crossing. Journal of Hydraulic Engineering. 125(6), pp. 645-651. https://doi.org/10.1061/(ASCE)0733-9429(1999)125:6(645)

Joyce, H.M., Warburton, J. and Hardy, R.J. 2020. A catchment scale assessment of patterns and controls of historic 2D river planform adjustment. Geomorphology. 354, pp. 107046. https://doi.org/10.1016/j.geomorph.2020.107046

Khan, S. and Fryirs, K. 2020. An approach for assessing geomorphic river sensitivity across a catchment based on analysis of historical capacity for adjustment. Geomorphology. 359, pp. 107135. https://doi.org/10.1016/j.geomorph.2020.107135

996 Khorram, S., Van der Wiele, C.F., Koch, F.H., Nelson, S.A. and Potts, M.D. 2016. Principles of applied remote
997 sensing. Springer International Publishing.

998 Kirby, A., Roca, M., Kitchen, A., Escarameia, M. and Chesterton, O. 2015. Manual on scour at bridges and
999 other hydraulic structures (C742). Construction Industry Research and Information Association.
1000 https://www.ciria.org/Resources/Free_publications/manual_on_scour.aspx

1001 Kondolf, G.M. and Piégay, H. 2016. Tools in fluvial geomorphology. John Wiley & Sons.
1002 https://doi.org/10.1002/9781118648551

1003 Lagasse, P.F., Spitz, W J., Zevenbergen L.W. and Zachmann, D.W. 2004. Handbook for predicting stream
1004 meander migration. The National Academies Press. https://doi.org/10.17226/23346.

1005 Lagasse, P.F., Zevenbergen, L.W., Spitz, W. and Arneson, L.A. 2012. Stream stability at highway structures
1006 (No. FHWA-HIF-12-004). U.S. Federal Highway Administration.

1007 Lamb, R., Aspinall, W., Odbert, H. and Wagener, T. 2017. Vulnerability of bridges to scour: insights from an
1008 international expert elicitation workshop, Natural Hazards Earth System Sciences. 17, pp. 1393-1409.
1009 https://doi.org/10.5194/nhess-17-1393-2017

1010 Latrubesse, E.M., Stevaux J.C. and Sinha, R. 2005. Tropical Rivers. Geomorphology. 70(3-4), pp. 187-206.
1011 https://doi.org/10.1016/j.geomorph.2005.02.005

1012 Lin, C., Han, J., Bennett, C. and Parsons, R.L. 2014. Case history analysis of bridge failures due to scour.
1013 International Symposium of Climatic Effects on Pavement and Geotechnical Infrastructure 2013. pp. 204-
1014 216. https://doi.org/10.1061/9780784413326.021

1015 Lisenby, P.E. and Fryirs, K.A. 2016. Catchment-and reach-scale controls on the distribution and expectation
1016 of geomorphic channel adjustment. Water Resources Research. 52(5), pp. 3408-3427.
1017 https://doi.org/10.1002/2015WR017747

1018 Lisenby, P.E., Fryirs, K.A. and Thompson, C.J. 2020. River sensitivity and sediment connectivity as tools for
1019 assessing future geomorphic channel behavior. International Journal of River Basin Management. 18(3), pp.
1020 279-293. https://doi.org/10.1080/15715124.2019.1672705

1021 Long, J.B. and Giri, C. 2011. Mapping the Philippines' mangrove forests using Landsat imagery. Sensors.
1022 11(3), pp. 2972-2981. https://doi.org/10.3390/s110302972

1023 Maddison, B. 2012. Scour failure of bridges. Proceedings of the Institution of Civil Engineers-Forensic
1024 Engineering, 165(1), pp. 39-52. https://doi.org/10.1680/feng.2012.165.1.39

1025 Maniatis, G., Williams, R.D., Hoey, T.B., Hicks, J. and Carroll, W. 2020. A decision support tool for assessing
1026 risks to above-ground river pipeline crossings. Proceedings of the Institution of Civil Engineers - Water
1027 Management, 173, pp. 87-100. https://doi.org/10.1680/jwama.18.00054

1028 McLean, D.G., Vasquez, J., Oberhagemann, K. and Sarker, M. 2012. Padma River morphodynamics near
1029 Padma Bridge. River Flow 2012 - Proceedings of the International Conference on Fluvial Hydraulics. 1. pp.
1030 741-747.

1031 Melville, B.W. and Coleman, S.E. 2000. Bridge scour. Water Resources Publication.

1032 Mosselman, E. 2006. Bank Protection and River Training Along the Braided Brahmaputra–Jamuna River,
1033 Bangladesh. In Sambrook Smith, G.H., Best, J.L., Bristow C.S. and Petts, G.E. (Eds), Braided Rivers: Process,
1034 Deposits, Ecology and Management. Blackwell. https://doi.org/10.1002/9781444304374.ch13

1035 Nelson, A. and Dubé, K. 2016. Channel response to an extreme flood and sediment pulse in a mixed
1036 bedrock and gravel-bed river. Earth Surface Processes and Landforms. 41, pp. 178-195.
1037 https://doi.org/10.1002/esp.3843

1038 Nguyen, U.N.T., Pham, L.T.H. and Dang, T.D. 2019. An automatic water detection approach using Landsat 8
1039 OLI and Google Earth Engine cloud computing to map lakes and reservoirs in New Zealand. Environmental
1040 Monitoring and Assessment. 191. pp. 235. https://doi.org/10.1007/s10661-019-7355-x

1041 Nones, M., Pugliese, A., Domeneghetti, A. and Guerrero, M. 2018. Po River morphodynamics modelled with
1042 the open-source code iRIC. In: Kalinowska M., Mrokowska M., Rowiński P. (eds) Free Surface Flows and
1043 Transport Processes. GeoPlanet: Earth and Planetary Sciences (pp. 335-346). https://doi.org/10.1007/978-
1044 3-319-70914-7_22

1045 Olsson, J., 2009. Improved road accessibility and indirect development effects: evidence from rural
1046 Philippines. Journal of Transport Geography. 17(6), pp.476-483.
1047 https://doi.org/10.1016/j.jtrangeo.2008.09.001

1048 Oo, M.M., Kyi, C.C.T. and Zin, W.W., 2019. Historical Morphodynamics Assessment in Bridge Areas using
1049 Remote Sensing and GIS Techniques. Civil Engineering Journal, 5(11), pp.2515-2524.
1050 https://doi.org/10.28991/cej-2019-03091429

1051 Ozcan, O. and Ozcan, O. 2019. Effect of hydrogeomorphological changes in flood plain on bridge multi-
1052 hazard performance. Fresenius Environmental Bulletin. 28(2), pp. 956-962.

1053 Panici, D., Kripakaran, P., Djordjević, S. and Dentith, K. 2020. A practical method to assess risks from large
1054 wood debris accumulations at bridge piers. Science of The Total Environment. 728, pp.138575.
1055 https://doi.org/10.1016/j.scitotenv.2020.138575

1056 Pregnolato, M. 2019. Bridge safety is not for granted – A novel approach to bridge management.
1057 Engineering Structures. 196, pp. 1091932. https://doi.org/10.1016/j.engstruct.2019.05.035

1058 Rokni, K., Ahmad, A., Selamat, A., and Hazini, S. 2014. Water feature extraction and change detection using
1059 multitemporal Landsat imagery. Remote Sensing. 6(5), pp. 4173-4189. https://doi.org/10.3390/rs6054173

1060 Rodolfo, K.S., Lagmay, A.M.F., Eco, R.C., Herrero, T.M.L., Mendoza, J.E., Minimo, L.G. and Santiago, J.T.
1061 2016. The December 2012 Mayo River debris flow triggered by Super Typhoon Bopha in Mindanao,
1062 Philippines: lessons learned and questions raised. Natural Hazards Earth System Sciences. 16, pp. 2683-
1063 2695. https://doi.org/10.5194/nhess-16-2683-2016

1064 Rouse, J.W., Haas, R.H., Schell, J.A., and Deering, D.W. 1974. Monitoring vegetation systems in the Great
1065 Plains with ERTS. NASA special publication, 351, pp. 309.

1066 Rowland, J.C., Shelef, E., Pope, P.A., Muss, J., Gangodagamage, C., Brumby, S.P. and Wilson, C.J. 2016. A
1067 morphology independent methodology for quantifying planview river change and characteristics from
1068 remotely sensed imagery. Remote Sensing of Environment. 184, pp. 212-228.
1069 https://doi.org/10.1016/j.rse.2016.07.005

1070 Ruiz-Villanueva, V., Piégay, H., Gurnell, A.M., Marston, R.A. and Stoffel, M. 2016. Recent advances
1071 quantifying the large wood dynamics in river basins: New methods and remaining challenges, Review of
1072 Geophysics. 54, pp. 611-652. https://doi:10.1002/2015RG000514

1073 Sarker, M.H. and Thorne, C.R. 2009. Morphological response of the Brahmaputra–Padma–Lower Meghna
1074 river system to the Assam Earthquake of 1950. In Sambrook Smith, G.H., Best, J.L., Bristow C.S. and Petts,
1075 G.E. (Eds), Braided Rivers: Process, Deposits, Ecology and Management (pp. 289-310). Blackwell.
1076 https://doi.org/10.1002/9781444304374.ch14

1077 Schumann, G., Bates, P.D., Horritt, M.S., Matgen, P. and Pappenberger, F. 2009. Progress in integration of
1078 remote sensing–derived flood extent and stage data and hydraulic models. Reviews of Geophysics. 47(4),
1079 pp. RG4001. https://doi.org/10.1029/2008rg000274

1080 Schwanghart, W. Scherler, D. 2014. TopoToolbox 2 – MATLAB-based software for topographic analysis and
1081 modeling in Earth surface sciences. Earth Surface Dynamics. 2, pp. 1-7. https://doi.org/10.5194/esurf-2-1-
1082 2014

1083 Schwenk, J., Khandelwal, A., Fratkin, M., Kumar, V. and Foufoula-Georgiou, E. 2017. High spatiotemporal
1084 resolution of river planform dynamics from Landsat: The RivMAP toolbox and results from the Ucayali
1085 River. Journal of Geophysical Research: Earth and Space Science. 4(2), pp. 46-75.
1086 https://doi.org/10.1002/2016ea000196

1087 Scottish Environment Protection Agency, SEPA. 2010. Engineering in the water environment: good practice
1088 guide. River crossings. WAT-SG-25. 2nd Edition. Available online:
1089 https://www.sepa.org.uk/media/150919/wat_ps_06_02.pdf

1090 Sear, D., Newson, M., Hill, C., Old, J. and Branson, J. 2009. A method for applying fluvial geomorphology in
1091 support of catchment-scale river restoration planning. Aquatic Conservation: Marine and Freshwater
1092 Ecosystems 19(5), pp. 506-519. https://doi.org/10.1002/aqc.1022.

1093 Shuker, L.J., Gurnell, A.M., Wharton, G., Gurnell, D.J., England, J., Finn Leeming, B.F. and Beach, E. 2017.
1094 MoRPh: a citizen science tool for monitoring and appraising physical habitat changes in rivers. Water and
1095 Environment Journal 31(3), pp. 418–424. https://doi.org/10.1111/wej.12259.

1096 Shean, D.E., Alexandrov, O., Moratto, Z.M., Smith, B.E., Joughin, I.R., Porter, C. and Morin, P. 2016. An
1097 automated, open-source pipeline for mass production of digital elevation models (DEMs) from very-high-
1098 resolution commercial stereo satellite imagery. ISPRS Journal of Photogrammetry and Remote Sensing. 116,
1099 pp. 101-117. https://doi.org/10.1016/j.isprsjprs.2016.03.012

1100 Simon, A. and Downs, PW., 1995. An interdisciplinary approach to evaluation of potential instability in
1101 alluvial channels. Geomorphology. 12(3), pp. 215-232. https://doi.org/10.1016/0169-555X(95)00005-P

1102 Sinha R. and Latrubesse, E.M. 2020. Geomorphology of fluvial systems: Focus on tropical rivers,
1103 Geomorphology. 363, pp. 107223. https://doi.org/10.1016/j.geomorph.2020.107223

1104 Smith, M.J. and Pain, C.F. 2009. Applications of remote sensing in geomorphology. Progress in Physical
1105 Geography: Earth and Environment. 33(4), pp. 568-582. https://doi.org/10.1177/0309133309346648

1106 Spada, D., Molinari, P., Bertoldi, W., Vitti, A. and Zolezzi, G. 2018. Multi-Temporal Image Analysis for Fluvial
1107 Morphological Characterization with Application to Albanian Rivers. ISPRS Int. J. Geo-Inf . 7(8), pp. 314.
1108 https://doi.org/10.3390/ijgi7080314

1109 Strahler, A.N. 1957. Quantitative analysis of watershed geomorphology. Eos, Transactions American
1110 Geophysical Union. 38(6), pp. 913-920.

1111 Syvitski, J.P., Cohen, S., Kettner, A.J. and Brakenridge, G.R. 2014. How important and different are tropical
1112 rivers? An overview. Geomorphology. 227, pp. 5-17. https://doi.org/10.1016/j.geomorph.2014.02.029

1113 Thorne, C.R., Allen, R.G. and Simon, A. 1996. Geomorphological river channel reconnaissance for river
1114 analysis, engineering, and management. Transactions of the Institute of British Geographers. 21(3), pp.
1115 469-483. https://doi.org/10.2307/622592

1116 Timpe, K. and Kaplan, D. 2017. The changing hydrology of a dammed Amazon. Science Advances. 3(11), pp.
1117 e1700611. https://doi.org/10.1126/sciadv.1700611

1118 Tolentino, P.L.M., Poortinga, A., Kanamaru, H., Keesstra, S., Maroulis, J., David, C.P.C. and Ritsema, C.J.
1119 2016. Projected Impact of Climate Change on Hydrological Regimes in the Philippines. PLOS ONE, 11, pp.
1120 e0163941. https://doi.org/10.1371/journal.pone.0163941

1121 Trueheart, M.E., Dewoolkar, M.M., Rizzo, D.M., Huston, D. and Bomblies, A. 2020. Simulating hydraulic
1122 interdependence between bridges along a river corridor under transient flood conditions. Science of The
1123 Total Environment. 699, pp. 134046. https://doi.org/10.1016/j.scitotenv.2019.134046

1124 Vallejo, S.C. 2015. Evaluation of Major Bridges in Cagayan Valley, Philippines. The Countryside Development
1125 Research Journal. 3(1): 13-18.

1126 Vasquez, J.A., McLean, D.G., O'Connor, V.F. and Zimmermann, A. 2012. Hydraulic modeling for the Padma
1127 River Bridge. River Flow 2012 - Proceedings of the International Conference on Fluvial Hydraulics. pp. 1227-
1128 1233.

1129 Villafuerte II, M.Q., Macadam, I., Daron, J., Katzfey, J., Cinco, T. A., Ares, E.D. and Jones, R.G. 2020.
1130 Projected changes in rainfall and temperature over the Philippines from multiple dynamical downscaling
1131 models. International Journal of Climatology. 40, pp. 1784-1804. https://doi.org/10.1002/joc.6301

1132 Villafuerte II, M.Q., Matsumoto, J. and Kubota, H. 2015. Changes in extreme rainfall in the Philippines
1133 (1911–2010) linked to global mean temperature and ENSO. International Journal of Climatology. 35, pp.
1134 2033-2044. https://doi.org/10.1002/joc.4105

1135 Wang, C., Yu, X. and Liang, F. 2017. A review of bridge scour: mechanism, estimation, monitoring and
1136 countermeasures. Natural Hazards. 87, pp. 1881-1906. https://doi.org/10.1007/s11069-017-2842-2

Werbylo, K.L., Farnsworth, J.M., Baasch, D.M. and Farrell, P.D. 2017. Investigating the accuracy of photointerpreted unvegetated channel widths in a braided river system: a Platte River case study. Geomorphology, 278, pp. 163-170. https://doi.org/10.1016/j.geomorph.2016.11.003

West, A.J., Lin, C.W., Lin, T.C., Hilton, R.G., Liu, S.H., Chang, C.T., Lin, K.C., Galy, A., Sparkes, R.B. and Hovius, N., 2011. Mobilization and transport of coarse woody debris to the oceans triggered by an extreme tropical storm. Limnology and oceanography, 56(1), pp. 77-85. https://doi.org/10.4319/lo.2011.56.1.0077

Williams, R.D., Brasington, J. and Hicks, D.M. 2016. Numerical modelling of braided river morphodynamics: Review and future challenges. Geography Compass. 10(3), pp. 102-127. https://doi.org/10.1111/gec3.12260

World Bank. 2018. Philippines Economic Update, October 2018: Staying in the Course Amid Global Uncertainty. World Bank. https://doi.org/10.1596/30564

Woznicki, S.A., Baynes, J., Panlasigui, S., Mehaffey, M. and Neale, A. 2019. Development of a spatially complete floodplain map of the conterminous United States using random forest. Science of the Total Environment. 647, pp. 942-953. https://doi.org/10.1016/j.scitotenv.2018.07.353

Wulder, M.A. and Coops, N.C. 2014. Satellites: Make Earth observations open access. Nature, 513(7516), pp. 30. https://doi.org/10.1038/513030a

Xu, H. 2006. Modification of normalised difference water index (NDWI) to enhance open water features in remotely sensed imagery. International Journal of Remote Sensing. 27(14), pp. 3025-3033. https://doi.org/10.1080/01431160600589179

Yang, X., Pavelsky, T. M., Allen, G. H. and Donchyts, G. 2019. RivWidthCloud: An Automated Google Earth Engine Algorithm for River Width Extraction From Remotely Sensed Imagery. IEEE Geoscience and Remote Sensing Letters. 17(2), pp. 217-221. https://doi.org/10.1109/LGRS.2019.2920225

Zou, Z., Xiao, X., Dong, J., Qin, Y., Doughty, R.B., Menarguez, M.A., Zhang, G. and Wang, J. 2018. Divergent trends of open-surface water body area in the contiguous United States from 1984 to 2016. Proceedings of the National Academy of Sciences. 115(15), 3810-3815. https://doi.org/10.1073/pnas.1719275115